



**Optogenetic stimulation of AVP neurons in the anterior hypothalamus
promotes wakefulness**

**Optogenetische Stimulation von AVP Neuronen im vorderen
Hypothalamus induziert Wachheit**

Doctoral thesis for a medical doctoral degree
at the Graduate School of Life Sciences,
Julius-Maximilians-Universität Würzburg,
Section Neuroscience

submitted by

Florian Rumpf

from

Münchberg

Würzburg, 2022





**Optogenetic stimulation of AVP neurons in the anterior hypothalamus
promotes wakefulness**

Doctoral thesis for a medical doctoral degree at the Graduate School of Life Sciences,
Julius-Maximilians-Universität Würzburg, Section Neuroscience

Submitted by **Florian Rumpf** on:

Office Stamp

Members of the Thesis Committee:

Chairperson:	Prof. Dr. Stefan Störk
Primary Supervisor:	Prof. Dr. Charlotte Förster
Supervisor (Second):	Prof. Dr. Carmen Villmann
Supervisor (Third):	Prof. Dr. Michihiro Mieda
Date of Public Defense:	
Date of Receipt of Certificates:	

Affidavit

I hereby confirm that my thesis entitled “Optogenetic stimulation of AVP neurons in the anterior hypothalamus promotes wakefulness” is the result of my own work. I did not receive any help or support from commercial consultants. All sources and / or materials applied are listed and specified in the thesis.

Furthermore, I confirm that this thesis has not yet been submitted as part of another examination process, neither in identical nor similar form.

Würzburg, 12th of December 2022

Florian Rumpf

Eidesstaatliche Erklärung

Hiermit erkläre ich an Eides statt, die Dissertation „Optogenetic stimulation of AVP neurons in the anterior hypothalamus promotes wakefulness“ eigenständig, d.h. insbesondere selbständig und ohne Hilfe eines kommerziellen Promotionsberaters, angefertigt und keine anderen als die von mir angegebenen Quellen und Hilfsmittel verwendet zu haben.

Ich erkläre außerdem, dass die Dissertation weder in gleicher noch in ähnlicher Form bereits in einem anderen Prüfungsverfahren vorgelegen hat.

Würzburg, 12. Dezember 2022

Florian Rumpf

Table of contents

Introduction.....	1
The suprachiasmatic nucleus (SCN): the circadian pacemaker of the brain	1
A closer look at the SCN in mammals and the neuron populations within	2
Lessons learned from the circadian clock in <i>Drosophila melanogaster</i>	3
The transcriptional post translational feedback loop in mammals (TTFL)	4
AVP neurons play a special role in the control of behavioral rhythmicity	7
Network Interactions in the SCN.....	7
Mechanisms underlying the sleep/wake cycle in mammals	8
Central modulation of sleep and activity in rodents	10
Aims and objective of the present study	11
Methods.....	13
Animals	13
Optogenetic Constructs for the Manipulation of the SCN.....	14
Strategy to express optogenetic probes.....	15
Introduction of the optogenetic construct and implant to transgenic mice	16
In vivo stimulation conditions	18
Sleep stage scoring and analysis	19
Markov chain transition analysis of sleep stages	20
Confirmation of opsin expression by immunohistochemistry	21
Electrophysiology	22

Statistical analysis.....	24
Results.....	25
Exploration of optimal conditions for the optogenetic SCN stimulation	25
Stabilized step function opsin (SSFO) in AVP-Cre mice promotes wakefulness	28
Markov chain sleep stage transition analysis.....	32
Electrophysiological function of stabilized step function opsin in AVP neurons	37
Discussion.....	41
Acknowledgements.....	51
Bibliography	52
Key resource table.....	63
Attachments	64
Equipment preparation.....	78
Mouse preparation	78
Fixture of mouse to stereotactic frame.....	78
Craniectomy.....	78
Needle preparation	79
Virus injection.....	79
Implant optic fiber.....	79
Implant EEG/EMG electrodes	79
Finalize implant	80
Appendix – CV	87

Table of figures

Figure 1: The known clock network of <i>Drosophila melanogaster</i>	4
Figure 2: The circadian gene network in mammals.....	5
Figure 3: Generation of Ayp-Cre mice.....	14
Figure 4: Implant sketches and mouse during surgery	17
Figure 5: Representative histochemistry of SCN slices.....	21
Figure 6: Illustration of the gross time schedule for the preliminary experiments.....	26
Figure 7: Experimental setup for preliminary experiments	26
Figure 8: Bar chart of the sleep stage distributions.....	27
Figure 9: Heatmap of the proportion of wakefulness in SSFO mice at baseline.....	28
Figure 10: Heatmap of the proportion of wakefulness in SSFO mice during stimulation	29
Figure 11: Heatmap of the proportion of wakefulness in control mice at baseline	30
Figure 12: Heatmap of the proportion of wakefulness in control mice during stimulation.....	30
Figure 13: Sleep stage distributions at baseline and stimulation in 20-minute bins.....	31
Figure 14: Sleep stage transition probabilities to wakefulness	33
Figure 15: Sleep stage transition probabilities to NREM	34
Figure 16: Sleep stage transition probabilities to REM.....	35
Figure 17: Transition probabilities with Welch's t-test.....	36
Figure 18: AVP neurons voltage clamp of optogenetic activation and inactivation	37
Figure 19: AVP neuron current clamp of optogenetic activation and inactivation	38
Figure 20: AVP neuron current clamp 20-minute continuous measurement	39

Summary

The mammalian central clock, located in the suprachiasmatic nucleus (SCN) of the anterior hypothalamus, controls circadian rhythms in behaviour such as the sleep-wake cycle. It is made up of approximately 20,000 heterogeneous neurons that can be classified by their expression of neuropeptides. There are three major populations: AVP neurons (arginine vasopressin), VIP neurons (vasoactive intestinal peptide), and GRP neurons (gastrin releasing peptide). How these neuronal clusters form functional units to govern various aspects of rhythmic behavior is poorly understood. At a molecular level, biological clocks are represented by transcriptional-posttranslational feedback loops that induce circadian oscillations in the electrical activity of the SCN and hence correlate with behavioral circadian rhythms. In mammals, the sleep wake cycle can be accurately predicted by measuring electrical muscle and brain activity. To investigate the link between the electrical activity of heterogeneous neurons of the SCN and the sleep wake cycle, we optogenetically manipulated AVP neurons in vivo with SSFO (stabilized step function opsin) and simultaneously recorded an electroencephalogram (EEG) and electromyogram (EMG) in freely moving mice. SSFO-mediated stimulation of AVP positive neurons in the anterior hypothalamus increased the total amount of wakefulness during the hour of stimulation. Interestingly, this effect led to a rebound in sleep in the hour after stimulation. Markov chain sleep-stage transition analysis showed that the depolarization of AVP neurons through SSFO promotes the transition from all states to wakefulness. After the end of stimulation, a compensatory increase in transitions to NREM sleep was observed. *Ex vivo*, SSFO activation in AVP neurons causes depolarization and modifies the activity of AVP neurons. Therefore, the results of this thesis project suggest an essential role of AVP neurons as mediators between circadian rhythmicity and sleep-wake behaviour.

Zusammenfassung (German Summary)

Die zentrale Uhr von Säugetieren, die sich im Nucleus suprachiasmaticus (SCN) des vorderen Hypothalamus befindet, steuert zirkadiane Verhaltensrhythmen wie den Schlaf-Wach-Rhythmus. Sie besteht aus etwa 20.000 heterogenen Neuronen, die nach ihrer Expression von Neuropeptiden klassifiziert werden können. Es gibt drei große Populationen: AVP-Neuronen, VIP-Neuronen und GRP-Neuronen. Wie diese Neuronengruppen funktionelle Einheiten bilden, um verschiedene Aspekte des rhythmischen Verhaltens zu steuern, ist nur unzureichend bekannt. Bei Säugetieren kann der Schlaf-Wach-Zyklus durch Messung der elektrischen Muskel- und Gehirnaktivität genau vorhergesagt werden. Um den Zusammenhang zwischen der elektrischen Aktivität heterogener Neuronen des SCN und dem Schlaf-Wach-Zyklus zu untersuchen, wurden AVP-Neuronen *in vivo* mit SSFO optogenetisch manipuliert und gleichzeitig ein Elektroenzephalogramm (EEG) und ein Elektromyogramm (EMG) bei frei beweglichen Mäusen aufgezeichnet. Die SSFO-vermittelte Stimulation von AVP-positiven Neuronen im vorderen Hypothalamus erhöhte den Gesamtanteil der Wachheit während der Stunde der Stimulation. Interessanterweise führte dieser Effekt zu einem Ansteigen des Schlafes in der Stunde nach der Stimulation. Eine Markov-Ketten-Analyse der Schlafphasenübergänge zeigte, dass die Depolarisierung der AVP-Neuronen durch SSFO den Übergang von allen Zuständen zum Wachsein fördert. Nach dem Ende der Stimulation wurde ein kompensatorischer Anstieg der Schlafphasenübergänge zum NREM-Schlaf beobachtet. *Ex vivo* verursachte die SSFO-Aktivierung in AVP-Neuronen eine Depolarisation und veränderte die Aktivität der AVP-Neuronen. Die Ergebnisse dieser Doktorarbeit könnten auf die Rolle der AVP-Neuronen als Vermittler zwischen zirkadianer Rhythmik und Schlaf-Wach-Verhalten hinweisen.

Introduction

The suprachiasmatic nucleus (SCN): the circadian pacemaker of the brain

The location of the circadian clock in mammals was identified by ablation studies (Moore and Eichler 1972, Stephan and Zucker 1972). Edgar et al. 1993 showed that SCN lesioned squirrel monkeys had a major disruption of their sleep/wake rhythm, sleep stages and drinking habits. Together, their total amount of sleep was increased, but the time spent in deep sleep phases was not altered (Edgar et al. 1993). This raised the question whether wakefulness was initiated and maintained by the SCN, opposed to the “need” for sleep that accumulates during the day. Conceptually, two additional models are possible: the circadian clock actively promotes sleep or, alternatively, the circadian clock actively promotes both sleep and wake in a circadian phase-dependent manner. As indicated by Mistlberger 2005 the conceptual model for a continuous influence by the SCN on the sleep/wake state had the most evidence. In this study, the present behavioral data of mammals and humans on circadian regulation of sleep was evaluated. The authors concluded that the role of the SCN is not restricted to an alerting function that opposes a sleep drive generated outside the SCN, but more likely has a profound and continuous influence on sleep and wake behavior throughout the circadian cycle. The species differences in the extent of the SCN engaging in the wake and sleep portions of the circadian rhythm explains the unique sleep increase observed in squirrel monkeys that could not be reproduced so far in other species (Mistlberger 2005). Most rodents show a bimodal activity rhythm. Being nocturnal animals, wakefulness can be observed during darkness with two activity peaks at the onset and at the end of the subjective night (dawn and dusk peaks of activity). During the day with lights on, rodents show low activity and spend most of their time sleeping (Cuesta et al. 2009). It may have become clear that the SCN actively promotes both sleep and wakefulness in rodents and humans, but it remains unclear how this is exactly facilitated.

A closer look at the SCN in mammals and the neuron populations within

The suprachiasmatic nucleus is formed by approximately 20,000 heterogeneous medial neurons in the anterior region of the murine hypothalamus. It sustains a 24-hour rhythm *in vivo* and *in vitro*. The presence of a circadian rhythmicity in the suprachiasmatic nucleus was first demonstrated by Schwartz and Grainer 1977 by studying the circadian rate of glucose consumption in the SCN. These authors already hypothesized that changes in glucose consumption are associated with altered functional neuronal activity (Schwartz and Gainer 1977). The rhythmic neuronal activity was confirmed by many subsequent studies (Inouye and Kawamura 1979) and would be maintained *in vitro*, thus confirming the presence of an autonomous circadian rhythm (Weaver 1998). This was followed by the identification of clock genes and their circadian expression as biochemical and molecular mechanisms that determine rhythmicity within the SCN (Weaver 1998). The SCN itself is formed by a heterogeneous population of neurons. Most neurons express GABA plus a dominant, name-giving neuropeptide and other minor neuromessengers (Herzog et al. 2017). The core region constitutes the ventrolateral part of the SCN and lies near the optic chiasm. Here multiple neuron populations are present; most importantly, VIP-neurons release vasoactive intestinal peptide and GRP-neurons produce gastrin-releasing peptide. This area receives dense retinal axonal projections through the retinohypothalamic tract of the eye and input from the midbrain raphe. The principal function of VIP neurons seems to be synchronization within the SCN. The shell of the SCN is the dorsomedial portion of the SCN and contains arginine vasopressin neurons (AVP neurons). In this region, inputs range from nonvisual cortical and subcortical afferents. AVP neurons play an important role in the pacemaking of the SCN. These neuron populations form a hierarchical circuit within the SCN that enables its function as a master clock. (Herzog et al. 2017)

Lessons learned from the circadian clock in *Drosophila melanogaster*

In the fruit fly *Drosophila melanogaster*, two clocks coexist and depend on each other: morning (M) and evening (E) oscillators. They separately control the activity of *Drosophila* in the morning and evening and thus play an important role in the adaptation of the circadian cycle to changes in the length of days. Tracking dawn and dusk, the activity of the fly can be adjusted to short winter or long summer days. The M and E oscillators have been partially tracked to distinct clock cells (Yoshii et al. 2012). Research in *Drosophila* also revealed that other properties, such as temperature can entrain the circadian clock. Such external or environmental cues that directly affect biological rhythms are called Zeitgebers (Tomioka and Yoshii 2006).

150 clock neurons have been identified in the brain of *Drosophila* that show oscillations of core clock genes. Four lateral and three dorsal neuronal groups can be identified (Figure 1), (Schubert et al. 2018). Among these, the large and small ventrolateral neurons (l-LN_v and s-LN_v) express the neuropeptide pigment dispersing factor (PDF). PDF is a signaling molecule that modulates other clock neurons by delaying the phase of their daily [Ca²⁺] oscillations (Liang et al. 2016, Liang et al. 2017). PDF is the VIP homolog in the mammalian central nervous system. The s-LN_v sustain rhythmicity in constant darkness (Helfrich-Forster 1998). Furthermore, they generate and time the morning activity peak and therefore are the morning oscillators as well as the main pacemakers of the circadian clock in *Drosophila*. The peak of activity in the evening is generated and controlled by the E cells. This is a heterogeneous group of cells formed by the 5th PDF lacking LN_v, the CRY⁺ LN_{ds} and some dorsal neurons. Research on *Drosophila melanogaster* also revealed the transcriptional post-translation feedback loop that formulates the circadian clock on a molecular basis (Huang 2018).

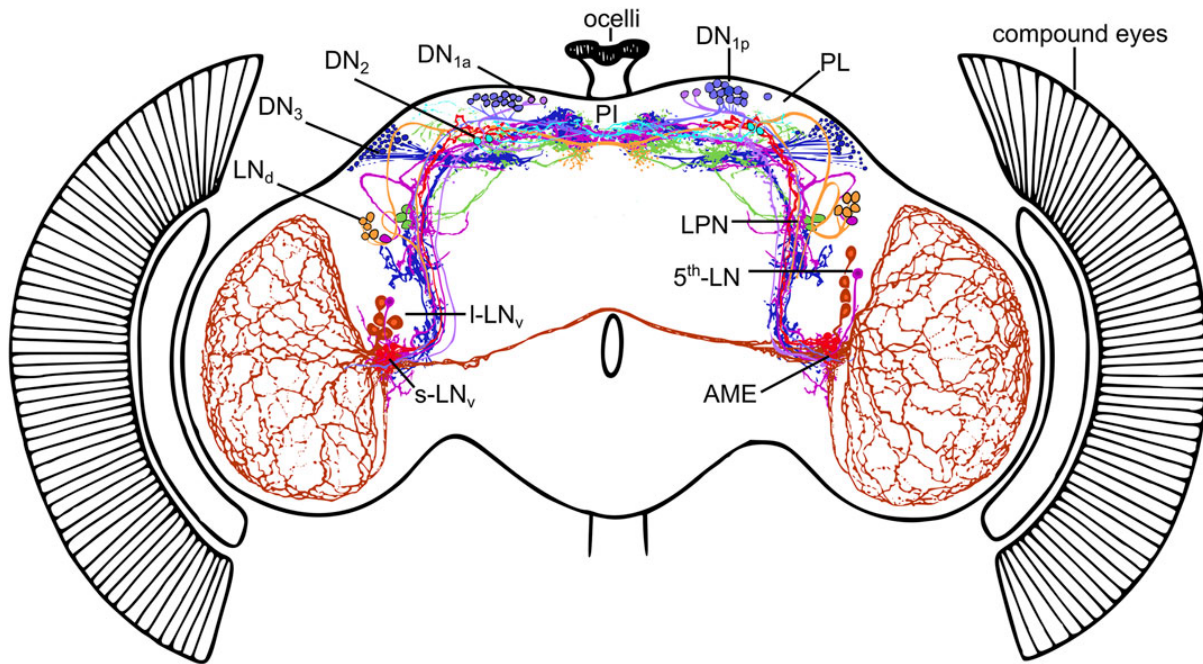


Figure 1: The known clock network of *Drosophila melanogaster*. Open-access figure from (Reinhard et al. 2022). Copyright 2022 Reinhard, Schubert, Bertolini, Hagedorn, Manoli, Sekiguchi, Yoshii, Rieger and Helfrich-Förster. Original caption: The clock network consists of Lateral Neurons (*s-LNvs*, *5th-LN*, *l-LNvs*, *LNds*, and *LPNs*) and Dorsal Neurons (*DN1as*, *DN1ps*, *DN2s*, *DN3s*), the neurites of which are highly connected. Many of them send fibers into the dorsal protocerebrum (including the neurosecretory centers in the pars intercerebralis (*PI*) and pars lateralis (*PL*)) as well as into the accessory medulla (*AME*) of both hemispheres, small neuropils at the base of the medulla. The *AME* can be regarded as the communication center of the clock neurons. Modified from Helfrich-Förster et al., 2007a with data from Schubert et al., 2018 and Reinhard et al., 2022 and this study.

The transcriptional post translational feedback loop in mammals (TTFL)

Similar to *Drosophila*, the circadian rhythm in mammals is generated by the interaction of clock genes with their encoded clock proteins. They form autoregulatory transcriptional post-translational feedback loops (TTFL), which generate the daily rhythm in individual cells (Nakamura 2012). The TTFLs control the circadian expression of clock genes in the SCN with several transcriptional regulators involved. Positive regulators have been identified as CLOCK and BMAL1, negative regulators as the period (PER) 1, 2 and 3 and cryptochrome (CRY) 1 and 2 proteins (Figure 2). The subjective day starts with the rise in the transcript levels of PER and CRY. This trend is enabled by binding of heterodimers of CLOCK and BMAL1 at an enhancer site (E-box) for PER and CRY. A build-up of PER and CRY levels is further mediated by translational regulation by an MAPK, mTOR, and eIF4E cascade. Later in the day, high concentrations of PER and CRY act as suppressors of CLOCK and BMAL1.

During the night, the transcript and protein levels of PER and CRY decrease again, as they lack the promotion by CLOCK and BMAL1. At the end of the night, their suppression of CLOCK and BMAL1 fades completely and a new cycle commences (Herzog et al. 2017).

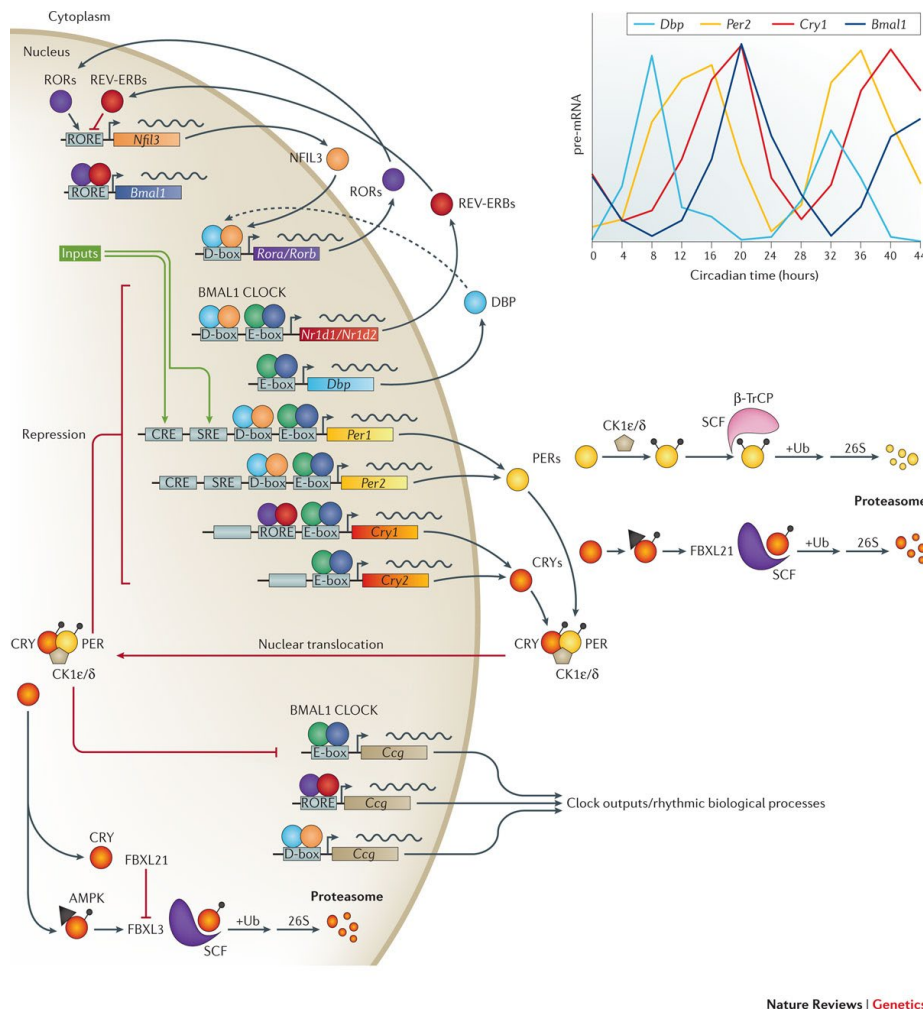


Figure 2: The circadian gene network in mammals. Reprinted with permission from Springer Nature Customer Service Centre GmbH: Springer NATURE REVIEWS GENETICS (Takahashi 2017), Copyright Springer Nature 2016. Original caption: At the core of the network, the basic helix–loop–helix (bHLH)–PER–ARNT–SIM (PAS) transcription factors CLOCK and BMAL1 activate the *Per1*, *Per2*, *Cry1* and *Cry2* genes, whose protein products interact and repress their own transcription. The stability of the period (PER) and cryptochrome (CRY) proteins are regulated by parallel E3 ubiquitin ligase pathways. CLOCK and BMAL1 also regulate the nuclear receptors REV-ERB α and REV-ERB β (encoded by *Nr1d1* and *Nr1d2*, respectively), which rhythmically repress the transcription of *Bmal1* and *Nfil3* (which encodes nuclear factor, interleukin-3 regulated) that is driven by the activators retinoic acid-related orphan receptor- α (ROR α) and ROR β (encoded by *Rora* and *Rorb*, respectively). NFIL3 in turn represses the PAR-bZip factor DBP (D-box binding protein) to regulate a rhythm in the ROR nuclear receptors. These three interlocked transcriptional feedback loops represent the three major transcriptional regulators of the majority of cycling genes. Different combinations of these factors generate different phases of transcriptional rhythms, as exemplified by the graph (top right) showing the RNA profiles of *Dbp*, *Per2*, *Cry1* and *Bmal1* in the mouse liver. Additional rhythmic output genes (so-called clock-controlled genes or Ccgs) are transcriptionally regulated by the three loops acting on E-boxes, RevDR2 and ROR-binding elements (ROREs) and D-boxes in the regulatory regions of target genes. AMPK, 5' AMP-activated protein kinase; CK1, casein kinase 1; CRE, cAMP response element; FBX, F-box protein; SCF, SKP1–cullin–F-box protein; SRE, serum response element; Ub, ubiquitin.

In this context, Xu et al. 2015 used crystal structures to analyze the binding sites of CRY1 responsible for the suppression. In CLOCK, a PAS domain and in BMAL1 a TAD domain were identified as the individual locations of CRY1 inhibition (Xu et al. 2015). Interestingly, already in 1998, it was discovered that most cells express clock genes similar to those of the SCN. The regional clock gene expression follows a tissue-specific circadian rhythm mirroring the mechanisms in the SCN (Balsalobre et al. 1998).

Furthermore, the TTFL is linked to the neuronal activity of the SCN and thereby also defines the period of the circadian rhythm neuronal activity. The SCN depolarization rate peaks in the middle of the day with a frequency of 4-10 Hz, in correlation with the rise in PER levels (Atkinson et al. 2011). Modification of transcription factors that results in the accumulation, degradation, or translocation of clock gene transcripts alter the rhythm. In mice, with the $CLOCK^{\Delta 19}$ mutant allele, the transcription promotion effect at the E-box was decreased. Heterozygotes had a longer circadian period, while homozygotes were arrhythmic (Partch et al. 2014). CLOCK-deficient mice on the other hand show a normal circadian rhythm which highlights the functional redundancy within the molecular clock (Debruyne et al. 2006). Phosphorylation of PER2 by Casein Kinases (CK) causes its degradation or stabilization depending on the target site of the CK. Therefore, CKs have a major influence on the intrinsic period of the clock by controlling the stability of PER2 and the complexes formed by CK (Partch et al. 2014). Furthermore, a mutation in CK1 δ that reduces enzymatic activity has profound consequences on sleep behavior in humans and results in the familial advanced sleep phase syndrome with a shorter circadian period (Xu et al. 2005).

AVP neurons play a special role in the control of behavioral rhythmicity

So far, the exact mechanism of the oscillations of the SCN output is unclear. No cell population, which orchestrates the pacemaking within the SCN to allow for a synchronized rhythm, has been identified (Webb et al. 2009). However, Mieda et al. 2015 studied BMAL1 knockout mice specifically in AVP neurons demonstrating a longer free-running period and an overall longer activity time of the behavior rhythm. Solely affecting one neuron population and thereby altering the circadian period gave evidence that the AVP neurons constitute a specific part in the pacemaking of the SCN. This fact was confirmed by AVP specific manipulation of Casein-Kinase1 δ . As expected, mice with CK1 δ deletion showed a longer free-running period and a shorter period in case of hyperexpression (Mieda et al. 2015, Mieda et al. 2016). Alternatively, lengthening the cellular period in VIP neurons through clock gene modification did not influence the *in vivo* period of the SCN (Lee et al. 2015). The debate about the differential roles of the shell and core of the SCN in pacemaking remains unsolved.

Network Interactions in the SCN

Throughout the day, variations in the sodium and potassium conductances of neurons most likely constitute the electrical activity of SCN neurons. Circadian changes in K⁺ channel expression are suggested to be the primary driver and mediate between TTFL and circadian oscillations (Whitt et al. 2016). An application of tetrodotoxin (TTX), which acts as an inhibitor of most voltage-gated Na⁺ channels, blocks the output of action potentials in the majority of neurons. The effect is not limited to the loss of SCN firing, which leads to a desynchronization of the network, but it also results in a decrease and disruption of circadian gene expression. This gives evidence for a bidirectional dependence of action potential firing rate and clock gene expression in the SCN (Enoki et al. 2012). One hypothesis to explain the bidirectional interconnection between electrical activity and clock gene expression is the intracellular

calcium level ($[Ca^{2+}]_i$). Voltage-gated $[Ca^{2+}]$ -channels and the release from intracellular storages facilitate the oscillation of $[Ca^{2+}]_i$ (Allen et al. 2017). The $[Ca^{2+}]_i$ rhythm correlates with the action potential rate and *Per* expression in SCN neurons (Brancaccio et al. 2013). The interplay of $[Ca^{2+}]_i$ levels and voltage rhythms was further analyzed in a cell-type-specific manner by Enoki et al. 2017. Voltage rhythms were proven to be synchronous over the network. However, $[Ca^{2+}]_i$ levels changed in a topological pattern with temporal differences in AVP and VIP neurons. Therefore, differently phased $[Ca^{2+}]_i$ levels express the regional-specific role of neuron populations (Enoki et al. 2017). Direct optogenetic depolarization or hyperpolarization of SCN neurons affected *Per* expression *in vitro* and locomotion *in vivo*. Jones et al. 2015 used an approach in which mouse lines were manipulated so that most neurons in the SCN expressed channelrhodopsin2 (ChR2) or halorhodopsin (NpHR). ChR2 or NpHR expression was facilitated under the control of an SCN-directed Cre driver (*Drd1a*) and verified by immunohistochemistry. *Ex vivo* optogenetic stimulation resulted in a phase shift in the circadian rhythm. C-FOS is a protooncogene that is expressed upon changes in neuronal activity and, thereby, can be used to detect the effects of exogenous factors on gene expression (Herdegen and Leah 1998). In the Jones et al. 2015 study, C-FOS immunohistochemistry showed increased gene expression in accordance with optogenetic stimulation. These changes were inhibited when TTX was applied to the slices. *In vivo*, ChR2 mice showed an activity onset provoked by optogenetic stimulation of SCN neurons (Jones et al. 2015).

Mechanisms underlying the sleep/wake cycle in mammals

The method used to record sleep predetermines the definition of sleep. In mammals and birds, sleep can be classified as non-rapid eye movement (NREM) sleep and rapid eye movement (REM) sleep. In these organisms, behavioral and electrophysiological measurements of sleep correlate with each other. Using EEG and EMG recordings, the

occurrence and depth of sleep can be efficiently monitored. Generally, sleep behavior is regulated by two mechanisms. The first one is called sleep homeostasis: the amount of previous awakening corresponds to the amount of sleep urge. This is explained by the production of sleep pressure that accumulates during the waking period. The driving force behind this is neuronal activity; however, there is no consensus on the details of this process. Concepts such as energy consumption due to neuronal activity, mechanisms related to neuronal plasticity, and sleep as a defense mechanism are currently discussed (Porkka-Heiskanen and Wigren 2020). Simultaneously, the second mechanism is the endogenous clock, which times sleep behavior and provides a circadian framework. Generally, the SCN drives circadian oscillations of electrical activity with high electrical activity during the day and low activity at night. Both of these mechanisms interact since sleep deprivation results in a decreased electrical activity of the SCN (Deboer et al. 2007).

Specific neuronal interaction and firing rhythms in the thalamocortical and hippocampus systems result in distinct oscillatory patterns in the EEG. Slow waves with a frequency of 1-4 Hz express the synchronized down states in cortical activity during NREM sleep (Vyazovskiy et al. 2009). Short waxing and waning of 9-15 Hz oscillations that originate in the thalamocortical system are called sleep spindles and can be mostly recorded during the transition of NREM to REM sleep (Sullivan et al. 2014). REM sleep is reflected by hippocampal theta oscillations. While these distinct patterns are merely the expression of the sleep states, the switches for the respective states have been identified and are located in deep subcortical circuits in the hypothalamus and brainstem (Weber 2017).

Central modulation of sleep and activity in rodents

Neuronal populations in the preoptic area of the anterior hypothalamus and the parafacial zone of the rostral medulla are active at sleep and have been associated with the initiation of sleep (Anaclet et al. 2014, Chung et al. 2017). The transition from NREM to REM sleep follows an ultradian rhythm with feedback control by areas in the hypothalamus and brainstem. REM-on and REM-off neurons that induce or inhibit REM sleep, respectively, have been identified. Most recently, such neurons have been found in the dorsomedial nucleus (DMH) of the hypothalamus. Neurons in the DMH that project to the preoptic area suppress REM and promote NREM sleep. On the contrary, neurons projecting to the raphe pallidus in the reticular formation of the brainstem promote REM and suppress NREM sleep (Chen et al. 2018). Wake-promoting neurons have been identified in the lateral hypothalamic area (LHA). Neurons that release orexin affect downstream centers of wakefulness in the dopaminergic ventral tegmental area, the noradrenergic locus coeruleus and the histaminergic tuberomammillary nucleus (Yamashita and Yamanaka 2017). In the LHA another neuronal population that releases melanin-concentrating hormone (MCH) has been confirmed to be REM-on neurons (Tsunematsu et al. 2014).

Various projections from the SCN to wake and sleep promoting areas in the brain have been identified. Sleep active neurons have been found in the preoptic area. Neuroanatomical studies indicated that the SCN output is relayed via the medial preoptic area, the subparaventricular zone or the dorsomedial hypothalamic nucleus to the preoptic area (Deurveilher and Semba 2005). Retrograde labeling exhibited that these projections predominantly reflect output from the shell of the SCN (Deurveilher et al. 2002). Preoptic GABAergic neurons projecting to the tuberomammillary nucleus have been shown to be both active during sleep phases and promote sleep upon optogenetic stimulation (Chung et al. 2017). Together, these findings hint towards a possible neuronal circuit linking the SCN and sleep promoting neurons.

Aims and objective of the present study

Recent years have demonstrated a better understanding of the neuroanatomical and molecular aspects of the master clock. Researchers have gained great insight into the qualities of the master clock. The location of the master clock has long been known, but how different neuron populations in the SCN operate in a synchronized circuit is not yet understood. Several studies observed its manifold characteristics such as: an integration of the retinal axonal projections conveying the light/dark signals, an *ex vivo* circadian activity that is maintained for a certain time, and compensation of the failure of parts of the network with a limited offset. All these qualities have underlying mechanisms in the circuitry of the SCN. Among many behavioral aspects such as feeding and drinking behavior, cortisol levels, and locomotor activity, sleep behavior is one of the most evident aspects that is governed by the SCN. This influence becomes especially tangible after a transatlantic flight when our sleep behavior is disrupted by jetlag. This common expression of circadian rhythm is easily observed, but so far it is unclear how the SCN imposes a circadian rhythm on our sleep and wake times.

For this thesis I proposed to investigate two main aims: (1) what is the role of AVP neurons in regulating the circadian activity, and (2) is the AVP neuronal activity the missing link between SCN and sleep behavior. To precisely manipulate certain neuronal populations in the SCN and thereby gain insights into the underlying circuitry, optogenetic experiments were carried out on an appropriate mouse model. First, I explored in small test groups the optimal conditions for stimulation of SCN neurons with respect to the effect on sleep behavior. Then I continued with the most promising conditions in a test group with an increased number of mice. The top candidates for the direct influence of the SCN on sleep behavior were AVP and VIP neurons. Both populations could have a dominant effect via downstream targets on the sleep wake cycle. VIP neurons could achieve this through higher synchronization of the network or AVP neurons through their influence on pacemaking.

Methods

Animals

Adult male mice (7 - 30 weeks old) were kept under standard light/dark cycle (12:12; lights on 08:45; lights off 20:45) with food and water ad libitum. Mice were maintained in individually ventilated cages (IVC) containing enrichment in a temperature- and humidity-controlled room. All experimental procedures involving animals were approved by the appropriate institutional Animal Care and Use Committee of Kanazawa University, Japan. The number of animals used is a minimum necessary to provide adequate data to test the hypotheses of this project. The number of animals required by the animal welfare committees was minimized wherever possible. The transgenic mice were kindly provided by Michihiro Mieda and his team.

Avp-Cre transgenic mice were originally designed by introduction of a bacterial artificial chromosome (BAC) that expresses Cre-recombinase under transcriptional control of the Avp promoter. To validate the localization of Cre activity, Avp-Cre mice were crossed with Rosa26-tdTomato reporter mice (Ai14 mice). In the offspring of these crossings, cells with Cre activity allowed the deletion of a loxP-flanked transcriptional blocker, which resulted in the expression of tdTomato. Cre activity was detected mainly in the suprachiasmatic nucleus (SCN), the supraoptic nucleus (SON), and the paraventricular nucleus (PVN) of the hypothalamus (Mieda et al. 2015). Furthermore, weaker Cre activity could be detected in some thalamic reticular neurons, granule cells of the dentate gyrus, the bed nucleus of the stria terminalis, and the inferior colliculus. Most of these regions have been reported to show some expression of Avp, suggesting that Cre expression in Avp-Cre mice mostly reflects endogenous expression of Avp. In the SCN, Cre activity was highly colocalized with AVP immunoreactivity with very little overlap of VIP immunoreactivity (Figure 3) (Mieda et al. 2015).

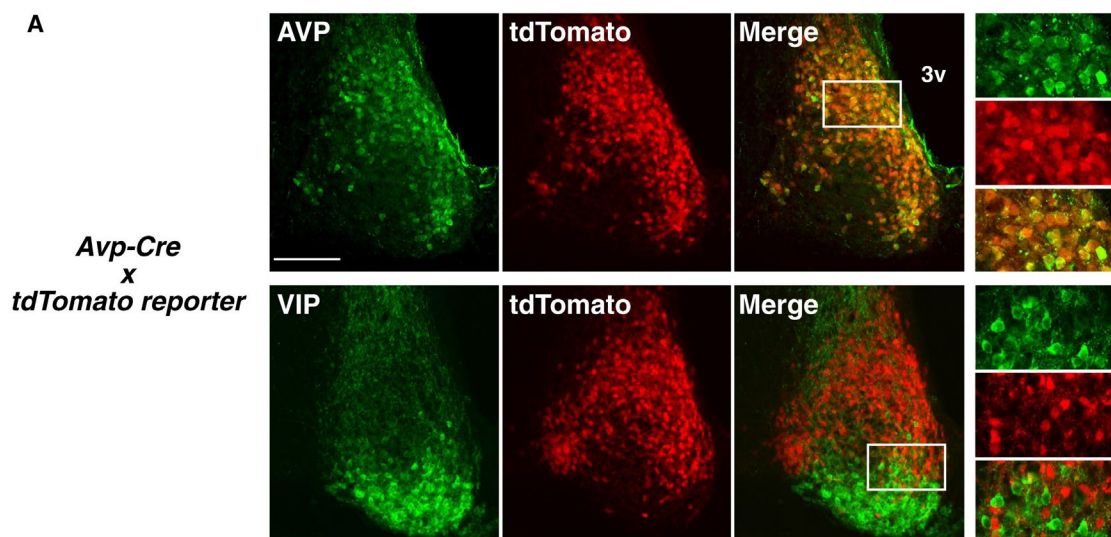


Figure 3: Generation of *Avp-Cre* mice. Cre-mediated recombination was specific to AVP neurons in the SCN of *Avp-Cre* mice crossed with *Rosa26-tdTomato* Cre-dependent reporter mice. Coronal brain sections were immunostained for AVP (upper row) or VIP (lower row) in green. Reprinted from *Neuron* Vol. 85, Michihiro Mieda, Daisuke Ono, Emi Hasegawa, Hitoshi Okamoto, Ken-ichi Honma, Sato Honma, Takeshi Sakurai, “Cellular Clocks in AVP Neurons of the SCN Are Critical for Interneuronal Coupling Regulating Circadian Behavior Rhythm”, Copyright (2015), with permission from Elsevier.

Optogenetic Constructs for the Manipulation of the SCN

Light-sensitive ion channels derived from algae are a well-established means to provide rapid electrical stimulation and reversibility in a cell-type-specific manner. Naturally, these so-called opsins are present in algal species such as *Chlamydomonas reinhardtii* (Channelrhodopsin-2 = ChR2), *Volvox carteri* (Channelrhodopsin-1 = VChR1), and *Natronomonas pharaonis* (Halorhodopsin). Generally, they share rapid kinetics when compared to other methods of manipulating neurons and can be effectively applied to control neural activity without disturbing physiological brain function (Nagel et al. 2003, Zhang et al. 2010).

In this study, two opsins were used: ChR2 H134R and SSFO (stabilized step function opsins). H134R is a point mutation of natural channelrhodopsin-2 that results in 2-3x enhanced cellular photocurrents while slowing down deactivation. The increased light sensitivity is crucial for the in vivo application (Williams et al. 2013).

SSFO is also a ChR2 variant that can be distinguished by two amino acid substitutions at C128S and D156A. Thereby, spontaneous deactivation kinetics are significantly slowed down, resulting in an open channel state with a time constant of nearly 30 minutes. A brief pulse of activating blue light initiates this process and the channel can be deactivated by a pulse of yellow light. These opsins induce a very stable photocurrent for the duration of their activation and can be used to depolarize neurons for a prolonged period. Furthermore, photoactivation can be facilitated by extremely low light intensity (Yizhar et al. 2011). Since various effects of SSFO on multiunit activity in neural circuits have been reported, I decided to perform an electrophysiological analysis to characterize the effect of SSFO in AVP neurons. The current literature suggests that SSFO can reduce ongoing synaptic activity and results in impaired information processing at the neuronal level (Yizhar et al. 2011).

Strategy to express optogenetic probes

To achieve effective control of cell electrical activity, high expression of opsin in target cells with proper integration into the cytoplasmic membrane is an important variable. To minimize the risk of low expression, I used a conditional viral expression system in this study. In general, various genetic strategies can be incorporated to facilitate high expression. Transgenic methods can be used to drive opsin expression in specific neuron populations conducted by their promoters. However, while being cell-specific, some promoters have a rather low transcriptional activity. Viral vectors have the advantage of achieving high levels of functional opsin and can be readily produced in biosafety level 1-certified tissue culture facilities within a few weeks. First, strong ubiquitous promoters were used to express Cre-recombinase in the targeted cells. Second, the optogenetic construct was packaged in a viral vector to effectively introduce it in vivo. The construct consists of the opsin, a marker for later detection in immunohistochemistry, and a transgenic switch (FLEX) that allows expression of

the opsin in cells with Cre recombinase only. I used a double-floxed inverted open-reading frame and thereby restricted the expression to AVP or VIP neurons in the experiments. This procedure resulted in selective and stable expression in cells of interest. Because some variation in the expression of opsin must always be expected and accurate injections are difficult to achieve, individual expression of opsin was verified in histological sections of the SCN after completion of the experiments. I opted for an adeno-associated virus (AAV) to act as vector for the optogenetic construct in the following experiments. After extraction, quantitative PCR was performed to measure the titer of the fabricated virus (A detailed protocol of the process and the results of the quantitative PCR can be found as attachments 1 and 2). In this study, the following constructs were used: AAV-EF1a-DIO-hChR2(H134R)-EYFP, AAV-DIO-mCherry, AAV-EF1a-DIO-SSFO-EYFP (Zhang et al. 2010).

Introduction of the optogenetic construct and implant to transgenic mice

Since the site of interest for the following experiments is a basal structure in the brain, stereotactic surgery is required to introduce the virus and the light delivery device. An integrated approach is to combine both procedures in one operation. This also reduces the stress inflicted on animals. Adult mice are suitable for the intervention. The surgery was performed in mice at the age of 3-7 months. First, the animals were injected intraperitoneally with a mixture of three anesthetics and analgesics: Medetomidine (trade name: Domitor), an $\alpha 2$ adrenergic agonist, Midazolam (trade name: Dormicum), a benzodiazepine and Butorphanol (trade name: Vetorphale), a synthetic opioid. Guided by a stereotaxic frame, the adeno-associated virus was injected via a Hamilton syringe. First, a small hole for the needle and optic fiber was made in the skull of the mice with a dental drill. The needle was inserted with visual control to ensure precision and avoid bending. After the needle had reached the injection site, 1 μ l of virus was slowly injected over a 10-minute period. The needle remained unmoved for

5 more minutes to avoid the injected solution from leaking out while the needle was removed. The needle was then pulled out and the optical fiber was inserted at the same site. This ensured co-location of light stimulus and injection site. Dental cement was applied to prevent any movement of the optical fiber. Between experiments, a dummy adaptor was used to protect the implant (Zhang et al. 2010). The central circadian clock influences various aspects of behavior, including feeding and drinking behavior, corticosterone levels, and locomotor activity. To record the effect of in vivo stimulation, a chronic measurement of one of these parameters is required. A precise and highly reliable behavior directed by the circadian rhythm is the sleep-wake cycle. The recording of an electroencephalogram (EEG) and an electromyogram (EMG) can provide accurate information on spontaneous activity and sleep stages. Therefore, mice also received an implant to record the electrical activity of the brain and the nuchal muscle. The injection of the optogenetic construct and the implantation of the optic fiber, EEG and EMG were all integrated into one surgical procedure. To overcome spatial challenges at the implantation site, the positioning of the EEG implant was slightly adjusted from the conventions (Figure 4). A detailed protocol of the procedure can be found in attachment 3 and a detailed implant map can be found as attachment 4.

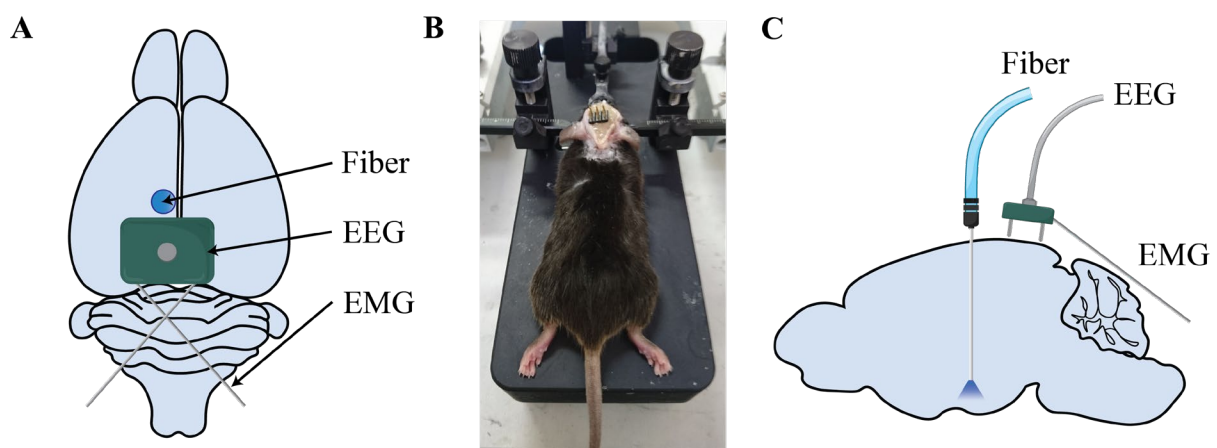


Figure 4: Implant sketches and mouse during surgery. Panel A gives the transverse layout of implants. It indicates the position of the optic fiber for optogenetic stimulation and electrodes for the EEG and EMG. Panel B shows a mouse during surgery. The orientation of the mouse reflects the layout of the schematic brain in panel A. Panel C shows the localization of the optic fiber and electrodes on the sagittal plane.

In vivo stimulation conditions

Multiple patterns of stimulation were executed. Mice were held under a 12:12 light/dark cycle with lights on at 8:45 and off at 20:45 in IVC housing. After surgery, mice were housed individually 1 week for healing in IVC housing and then moved to individual recording chambers for one more week of healing and habituation. Before the start of stimulation, the baseline EEG/EMG of mice was recorded. Afterwards mice were connected to the laser via an optic fiber and the recording of the EEG/EMG was started for the first stimulation (see attachment 5 for photos of the setup). For the recording of the EEG/EMG VitalRecorder from Kissei Comtec Co., Ltd. run on a windows computer was used. The recording was started at least one hour before the start of stimulation and continued for at least 6 hours. The following stimulation protocols were then carried out. For mice injected with ChR2, light was given for 1 h at a wavelength of 473 nm and 8 Hz. This resembles the protocol performed by Jones et al. (Jones et al. 2015). For mice injected with SSFO, light was given at a wavelength of 473 nm for 2 seconds for 3 times in one hour with no light in between for 20 minutes. Throughout this study, optic stimulation was performed with a blue-light laser that omitted light at a wavelength of 473 nm and an intensity of 10mW/mm². The intensity of the laser was regularly controlled with a handheld laser power meter (Edmund Optics Coherent LaserCheck) and adjusted accordingly. The operation of the laser was controlled using a single-board computer. This ensured consistent timing and manner of stimulations. Furthermore, it removed the experimenter from the experiment setting as a confounder for the behavior of mice. For ease of use, a Raspberry Pi was programmed to carry out this task. The corresponding programs written in Python can be found in attachments 6 and 7. Specific time points for stimulation were determined by the entrained rhythm of the mice. For these so-called Zeitgeber times (ZT), ZT0 is defined as lights on during the 12:12 light/dark cycle. Stimulation protocols were carried out at ZT13 and ZT5. Between each stimulation, mice were returned to IVC housing to rest for

at least 72 hours. This paradigm was only changed in control mice that were left to rest for at least 48 hours between the start of stimulations. The time windows described were chosen to track the effect of stimulation at two different times during the circadian rhythm in mice. Naturally around ZT13, one hour after lights have been turned off, the first activity peak can be observed. At ZT5 mice have a low activity level and spend most of the time phasing in and out of sleep.

Sleep stage scoring and analysis

The readout of the EEG/EMG was then scored using the SleepSign software from Kissei Comtec Co., Ltd. The recordings were trimmed to 6-hour windows: starting one hour before the start of stimulation, covering the full hour of stimulation, and continuing for 4 more hours after the end of stimulation. Then the recording was binned in 12 second epochs. Each epoch was assigned a stage during automatic screening of the data according to programmable logic. The assignable stages were W for wakefulness, R for REM sleep and N for NREM sleep. The logic used predefined boundary values for the EEG and EMG integrals, the theta wave ratio, and the delta wave ratio. These values had to be adjusted for each recording since the signal strength varied slightly depending on the recording chamber and implant. An example screening logic can be found in attachment 8. Finally, the screening was manually controlled and adjusted by the experimenter. To analyze the distribution of sleep stages, the recordings were further binned in 10-minute, 20-minute, or 1-hour intervals. This procedure allowed a comparison of the distribution of sleep stages between the hour of stimulation and the hours before and after stimulation. The baseline recordings were scored, binned, and analyzed in the same manner, allowing a comparison between the hour of stimulation and the hour at the corresponding Zeitgeber time at baseline.

Markov chain transition analysis of sleep stages

A discrete-time Markov chain model was fit on the previously scored sleep stage transition sequences. Sleep stage recordings were binned in 10-minute intervals and all recordings within a test group were aligned with their time stamps in a matrix. Since the original recordings were scored in 12 second epochs a maximum misalignment of 6 seconds between the recordings was to be expected. This also meant that every 10-minute time bin held 50 different stage observations and 49 stage transitions. The number of stage transitions was multiplied by the number of recordings that were included in the analysis (12) to receive the total number of sleep stage transitions analyzed per time bin (588). For easier computing, the sleep stages were encoded as numbers: 1 (= REM sleep), 2 (= non-REM sleep) and 3 (= wake). Afterwards, using the `markovchainFit` function one Markov chain was generated for all recordings within a 10-minute interval. Alas, the recordings within one time bin were treated as different observations of a phase transition at the same time stamp. This gave one 3 by 3 transition matrix for every time bin, reflecting the probabilities for a transition of the given states wake, REM, or non-REM sleep. Since the total length of each recording was 6 hours, this left 36 10-minute time bins for analysis. For a graphical representation of these numbers, one histogram for each possible phase transition was plotted, with the 36 time bins on the x axis and the state transition probabilities on the y axis. Since a transition from wake to REM sleep is unphysiological and would be only evident in diseases like narcolepsy the transition probability for such a behavior in all time bins was zero. Therefore, no histogram was plotted for the state transition from wake to REM sleep. These analyzes were carried out separately for the baseline and the stimulation recordings.

Confirmation of opsin expression by immunohistochemistry

To control the quality of the injections, immunohistochemical stainings were performed on all injected mice after the experiments had finished (Figure 5). Mice were deeply anesthetized with Avertin intraperitoneally. Mice were perfused by inserting a needle into the left ventricle. After flushing the vascular system with phosphate buffered saline (PBS), the mouse was perfused with 50 ml of 4% paraformaldehyde (PFA) in PBS. The mice brains were extracted and immersed in post-fixation solution (4% PFA) for 4 hours followed by 30% sucrose in PBS for 2 days at 4°C. Fixed brains were embedded in Sakura Tissue-Tek and cut using a cryostat microtome (Leica CM1860). 30 µm coronal slices were taken between the occipital end of the anterior commissure and the rostral end of the hippocampus. The slices were handled as floating sections in PBS.

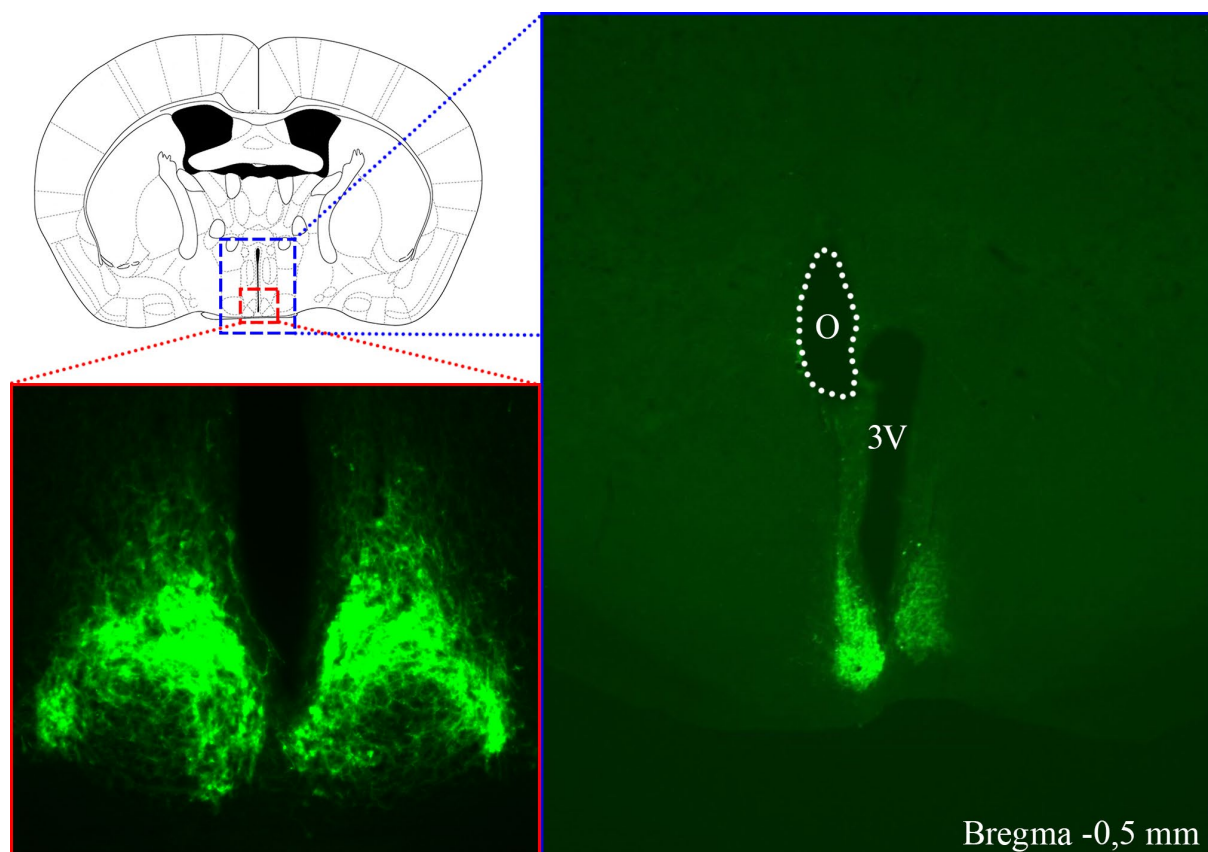


Figure 5: Representative histochemistry of SCN slices. Overview (blue box) and 10x magnification (red box) are mapped to a coronal mouse brain pictogram that the author abstracted from Paxinos mouse brain atlas. Expression of the opsin is limited to the SCN, while there was no expression at the paraventricular nucleus of the hypothalamus or the thalamic reticular nucleus. The marking caused by the optic fiber was located in close proximity to the SCN (O, white dotted outline). 3rd ventricle (3V) labelled as landmark.

For immunostaining, the sections were further washed in PBS with 0.3% Triton X-100 (PBST) and then blocked with a blocking solution (PBST plus 3% bovine serum albumin). Slices were incubated overnight with a rabbit anti-GFP antibody (1:1000, A11122, Thermo Fisher Scientific) as primary antibody in blocking solution at 4°C. After another round of washing in PBST, slices were incubated for 4h with Alexa Fluor 488-conjugated donkey anti-rabbit IgG (1:2000, A21206, Thermo Fisher Scientific) in blocking solution. After a last round of washing with PBS, the slices were mounted and air dried on glass slides. The mounted slices were covered with Vectashield HardSet mounting medium with DAPI (H-1500, Vector Laboratories). The blue counterstain of DAPI acts as a nuclear marker and allows for easy identification of cells. The expression of optogenetic constructs could then be identified with fluorescence microscopy (BZ-9000, Keyence and Fluoview Fv10i, Olympus). This is the case even without immunostaining, because the injected optogenetic vector contained the sequence of the green fluorescence protein EYFP (enhanced yellow fluorescent protein).

Electrophysiology

Single cell recordings of AVP neurons were made in SCN slices. Male mice at the age of 1 month were suitable for this kind of experiment. AVP-Cre mice that also specifically drive td-Tomato in AVP neurons were used. After receiving a stereotactic injection of pAAV-EF1a-DIO-SSFO-EYFP, the mice were housed in IVC housing to heal for 2 weeks. Although these experiments were performed *ex vivo*, it was critical to keep the cells alive as long as possible. Therefore, the collected tissue had to be kept in an adequate external solution. Two different solutions were prepared: cutting solution to collect the whole brain and slices, and recording solution to perform the electrophysiological recordings. Before use, these solutions were freshly prepared. During use, they were cooled whenever possible and infused with a carbogen

mixture of 95% O₂ and 5% CO₂ (see attachment 9 and 10 for the composition of external solutions). The entire brain was acutely collected from living mice anesthetized with isoflurane. The brains were then cut from caudal to rostral in cooled cutting solution using a vibratome (87 Hz). 250 μ m slices were collected between the rostral end of the hippocampus and the caudal end of the anterior commissure. Slices were then incubated for 30 minutes in cutting solution and 30 minutes in recording solution while being infused with the gas mixture. Slices collected in this manner were used for recording up to 8 hours after cutting. A fluorescent microscope was then used to confirm the expression and colocalization of the optogenetic construct with AVP neurons. After selecting the best section, it was placed in a glass well with recording solution on the patch clamp rig. An optic fiber connected to a LED laser was placed near the SCN. A glass electrode (from borosilicate glass capillaries with filament using a Sutter micropipette puller) was prepared and filled with internal solution (see attachment 11 for internal solution composition). It is then mounted on the manipulator holding the recording pipette and directed towards an AVP neuron expressing the optogenetic construct. Orange light (561 nm) was flashed on the slices to inactivate constitutive activation of SSFO. The cell was then patch-clamped.

Afterward, a whole-cell patch-clamp configuration was achieved by removing the cell membrane at the tip of the electrode. In the voltage clamp mode, the currents over the cell membrane were recorded. In current clamp mode, the voltage over the cell membrane was recorded. At baseline, a membrane potential of -20 mV could be observed in AVP neurons in SCN slices. The constitutive leakage of Na⁺ current in AVP neurons might have contributed to this shallow membrane potential. Another confounding factor could be the release of transmitters by the depolarization of SSFO, which directly affects the membrane potential. NMDA, AMPA, and GABA receptor blockers were added to the slices to eliminate this potential effect. The applied blockers were 25 mM APV ((2R)-amino-5-phosphonovaleric

acid), a competitive NMDA receptor antagonist, 10 mM CNQX (Cyanquixaline), a competitive AMPA receptor antagonist, and 10 mM bicuculline, a competitive GABA receptor antagonist. To achieve a membrane potential of -60 mV, a current of -30 to -100 pA was injected.

Statistical analysis

Data analysis, statistical computation, and graph plotting were performed exclusively with R version 4.0.3 (“Bunny-Wunnies Freak Out”). The scored sleep stages were handled as time series in tidy data frames (R packages “tidyverse” and “data.table”). Time variables were formatted with the R package “lubridate”. All graphs were created with the R package “ggplot2”, and color pallets and scales were imported from the R packages “scales” and “RColorBrewer”. Discrete-time Markov chain models were fitted with the R package “markovchain” on the raw sleep stage sequences. The node plots for Markov chain sleep stage transition probabilities were performed with the R package “DiagrammeR”. A pairwise comparison of transition probabilities was made using Welch’s t-test. The test statistic for this two-sample two-tailed test is given in Equation 1.

$$\text{Welch's t-test test statistic} = \frac{\bar{X}_1 - \bar{X}_2}{\sqrt{\frac{s_1^2}{n_1} + \frac{s_2^2}{n_2}}} \quad (1)$$

where \bar{X}_1 and \bar{X}_2 = sample means

n_1 and n_2 = sample sizes

s_1^2 and s_2^2 = sample variances

Results

Exploration of optimal conditions for the optogenetic SCN stimulation

The first sets of experiments were performed to explore the optimal conditions for further experimental series. The objective was to identify an effective and executable method to modify the sleep-wake behavior of mice. Previous research has shown that neuronal manipulation can have dramatic effects on behavior reflecting circadian rhythmicity (Chen et al. 2018). However, a link between behavior and the central circadian clock, the suprachiasmatic nucleus, has hardly been explored so far. For precise temporal and local manipulation of neurons, optogenetic stimulation was used. The measured parameters for the effect of the stimulation were EEG and EMG recordings. These recordings were then used to predict the stages of sleep of the animals during the recording times. To identify the optimal conditions for the optogenetic stimulation of the SCN, 4 groups of mice were tested. Each group consisted of two animals:

AVP mice injected with AAV-EF1a-hChR2(H134R)-EYFP

AVP mice injected with AAV-EF1a-DIO-SSFO-EYFP

VIP mice injected with AAV-EF1a-hChR2(H134R)-EYFP

VIP mice injected with AAV-EF1a-DIO-SSFO-EYFP

All mice received an implant consisting of an optic fiber and EEG/EMG electrodes. After the procedure, the mice showed no motor or behavioral impairments. They adapted well to the new environment of the recording chambers and showed normal levels of curiosity, exploring the new environment and testing its transparent walls. After the healing period, *in vivo* stimulations were performed. The time schedule and study design for this set of experiments are illustrated in Figures 6 and 7.

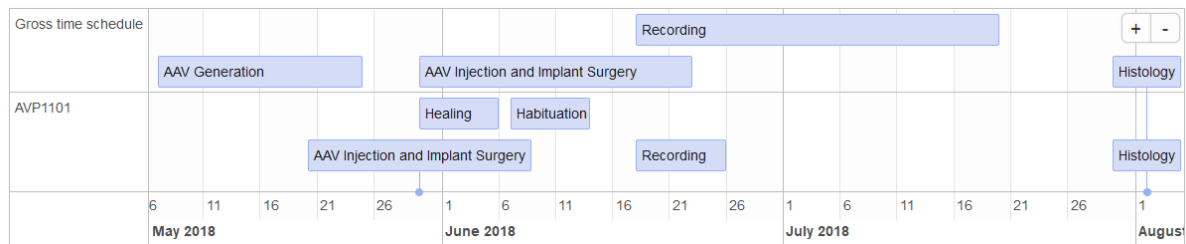


Figure 6: Illustration of the gross time schedule for the preliminary experiments and an exemplified timeline for one individual mouse

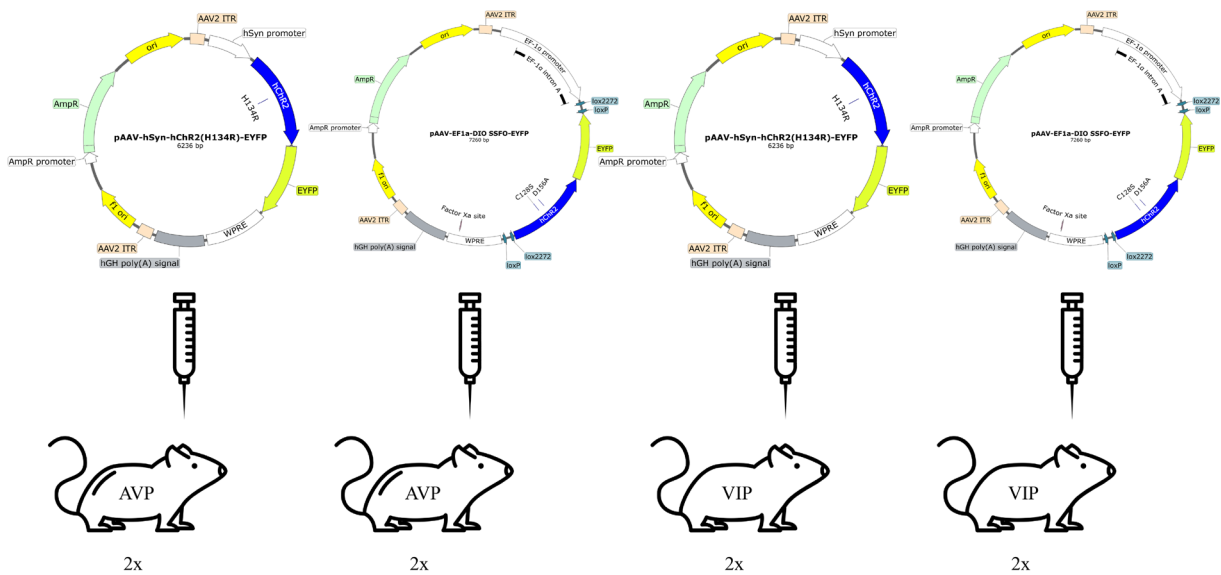


Figure 7: Experimental setup for preliminary experiments. The top part of the figure gives details for the used optogenetic constructs: AAV-EF1a-hChr2(H134R)-EYFP and AAV-EF1a-DIO-SSFO-EYFP. Below the mice lines and number of animals per experimental group are given. Syringe and mouse icon by Iconic from nounproject.com.

For each group of mice, experiments were carried out with a measurement duration of 6 hours at two specific Zeitgeber times (ZT). The first 6-hour surveyed period lasted from ZT4 to ZT10 (12:45-18:45 JST) and the second from ZT12 to ZT18 (20:45-02:45 JST). Optogenetic stimulations were then performed at ZT5 (light; sleep phase) and ZT13 (dark; awake phase). The results are shown in Figure 8: Each graph provides the sleep distribution for one indicative mouse from each group over a 6-hour period of measurement, binned into one-hour intervals.

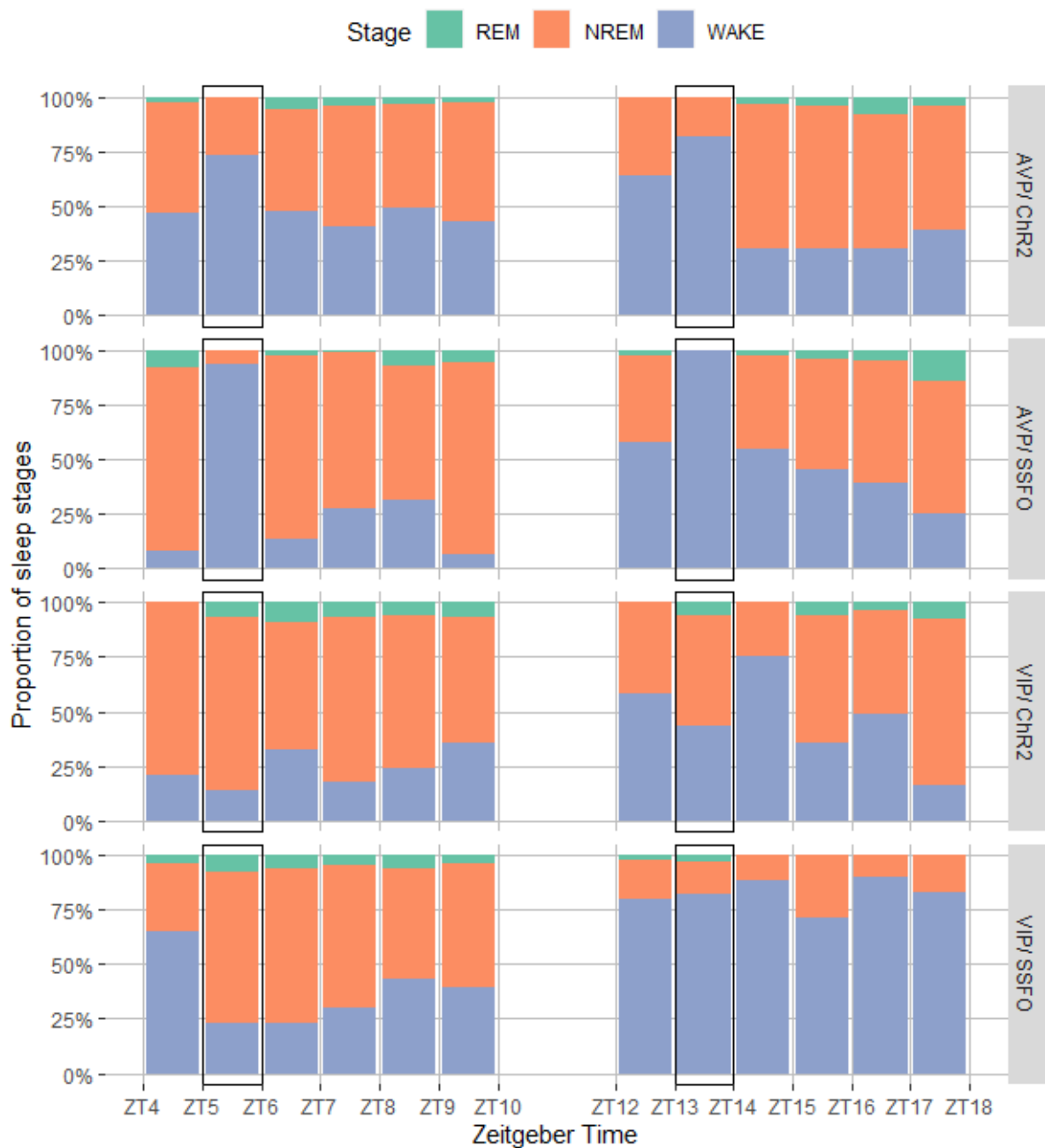


Figure 8: Bar chart of the sleep stage distribution for one indicative mouse from each of the 4 groups: Mice with the expression of pAAV-hSyn-hChr2(H134R)-EYFP in AVP neurons (AVP/ Chr2), mice with the expression of pAAV-EF1a-DIO-SSFO-EYFP in AVP neurons (AVP/ SSFO), mice with the expression of pAAV-hSyn-hChr2(H134R)-EYFP in VIP neurons (VIP/ Chr2), mice with the expression of pAAV-EF1a-DIO-SSFO-EYFP in VIP neurons (VIP/ SSFO). The figure is faceted into 4 rows according to these groups. The x-axis gives Zeitgeber Time (ZT) measured as the number of hours after the lighting in home cages is turned on as an external cue (Zeitgeber). The y-axis gives the proportion of sleep stages in percent (%). The bars are colored according to the proportion of sleep stages, which were defined as wakefulness (=WAKE, purple), non-rapid eye movement sleep (=NREM, red) and rapid eye movement sleep (=REM, green). Black boxes indicate the hour of stimulation.

Mice with expression of SSFO in AVP neurons showed a trend towards an increase in wakefulness during the hour of stimulation. This effect was unique compared to the other three groups of mice. Because no effect was observed in three groups of mice, we assumed that light-only stimulation of SCN neurons had no observable effect on wakefulness. However, these observations were rather uncertain considering the very small group sizes.

Stabilized step function opsin (SSFO) in AVP-Cre mice promotes wakefulness

To further narrow down the observed effects in mice expressing SSFO in AVP neurons, I repeated the experiments with a larger group size. In addition, a separate control group was used in these experiments. Nine AVP-Cre mice were injected with AAV-EF1a-DIO-SSFO-EYFP. A control group of mice consisted of two AVP-Cre mice injected with AAV-EF1a-hChR2(H134R)-EYFP and two AVP-Cre mice injected with AAV-DIO-mCherry¹. All mice received an optic fiber and an EEG/EMG implant.

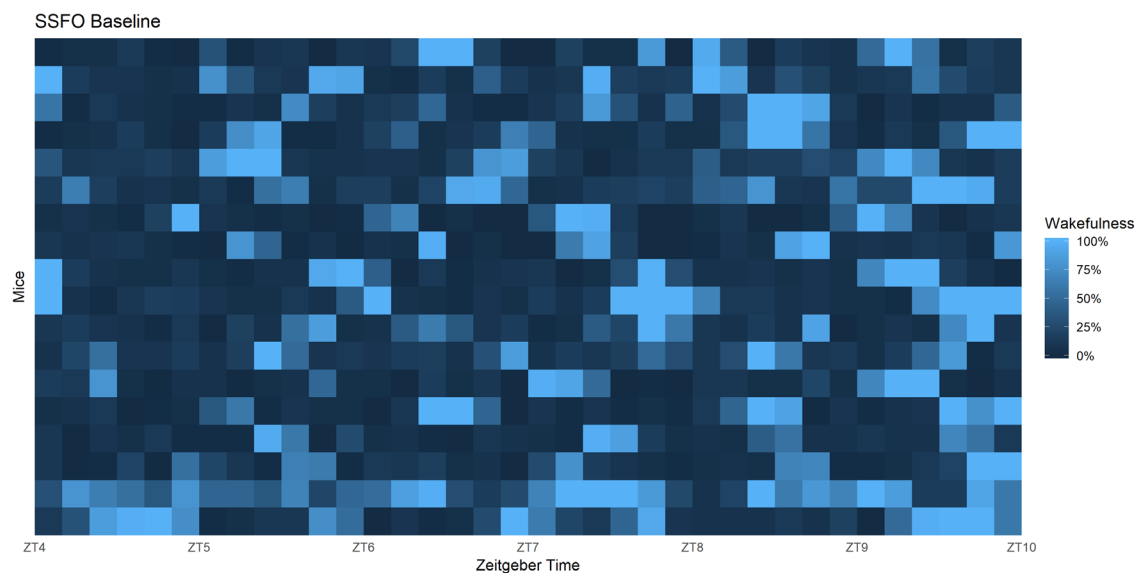


Figure 9: Heatmap of the proportion of wakefulness observed at baseline in mice with expression of AAV-EF1a-DIO-SSFO-EYFP in AVP neurons ($n=9$). Each row represents one measurement, with the squares spanning 10-minute time bins. The fill color of squares represents the proportion of wakefulness within each 10-minute time bin and ranges from light blue (high proportion of wakefulness) to dark blue (low proportion of wakefulness). The x-axis gives Zeitgeber Time (ZT) measured as the number of hours after the lighting in home cages is turned on as an external cue (Zeitgeber).

¹ Kindly provided by Yusuke Tsuno, Kanazawa University, Graduate School of Medical Science Department of Integrative Neurophysiology

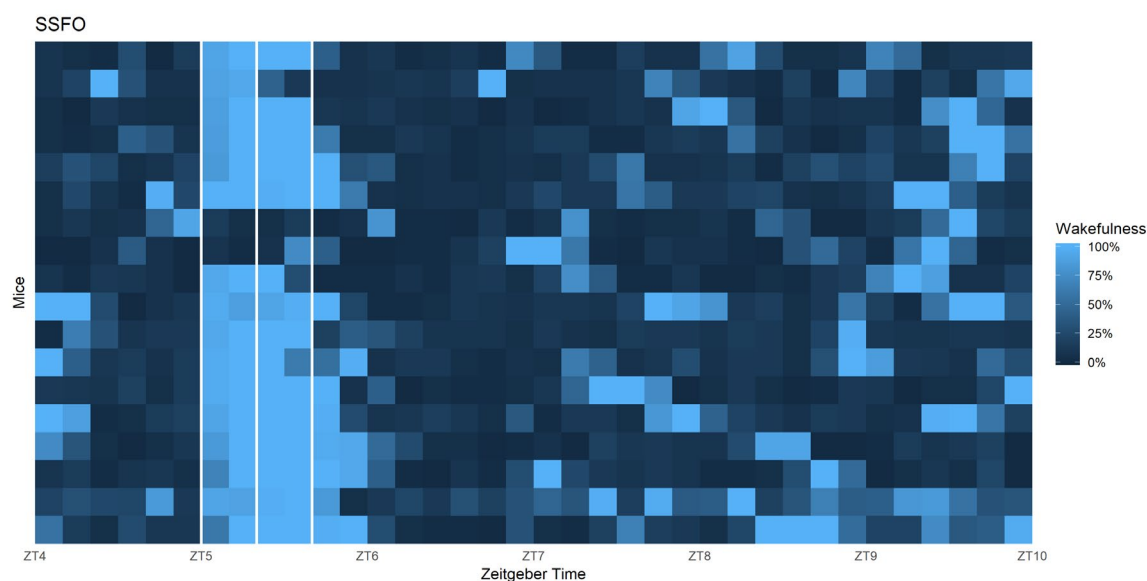


Figure 10: Heatmap of the proportion of wakefulness observed during, before and after stimulation of mice with expression of AAV-EF1a-DIO-SSFO-EYFP in AVP neurons ($n=9$). Each row represents one measurement, with the squares spanning 10-minute time bins. The fill color of squares represents the proportion of wakefulness within each 10-minute time bin and ranges from light blue (high proportion of wakefulness) to dark blue (low proportion of wakefulness). The x-axis gives Zeitgeber Time (ZT) measured as the number of hours after the lighting in home cages is turned on as an external cue (Zeitgeber). The white lines indicate the times of blue light exposure to the SCN.

After surgery and recovery, baseline measurements showed a physiological rhythm of activity in mice. Figure 9 is the graphic representation of the proportion of wakefulness for each mouse within 10-minute time intervals for the first 6-hour measuring period. Next stimulations and recording were carried out at exactly the same time as done in the preliminary experiments. For further analysis, measurements from the preliminary experiments were included. For each mouse and each surveyed period, at least two recordings were carried out. Figure 10 shows the proportion of wakefulness under stimulation conditions as a heat map. Each row represents one measurement, with the squares spanning 10-minute time bins. The proportion of wakefulness within each 10-minute time bin is colored as the fill of its square. Dark blue indicates a low proportion of wakefulness, and light blue indicates a high proportion of wakefulness.

Figures 9 and 10 still include mice that were later excluded from the analysis due to lack of opsin expression (e.g. rows 7 and 8 from the top). These results confirmed the

increased wakefulness initially observed during the hour of stimulation in mice expressing SSFO in AVP neurons. In some cases, the effect was also exhausted by the third application of light. Control mice, on the other hand, did not show any effect upon stimulation with blue light (see Figures 11 and 12). The results of the same experiments carried out in the second 6-hour period from ZT12 to ZT18 can be found in attachments 12 and 13.

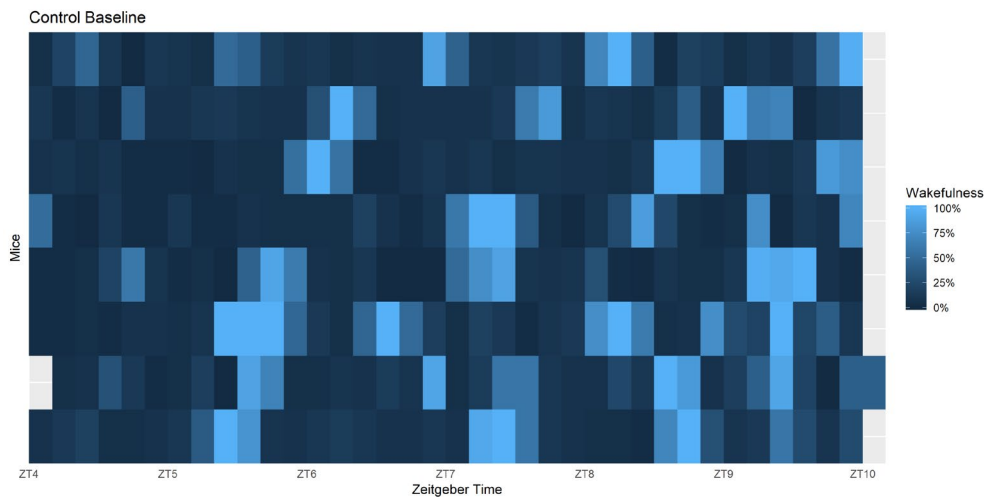


Figure 11: Heatmap of the proportion of wakefulness observed at baseline in the control group ($n=4$). Each row represents one measurement, with the squares spanning 10-minute time bins. The fill color of squares represents the proportion of wakefulness within each 10-minute time bin and ranges from light blue (high proportion of wakefulness) to dark blue (low proportion of wakefulness). The x-axis gives Zeitgeber Time (ZT) measured as the number of hours after the lighting in home cages is turned on as an external cue (Zeitgeber).

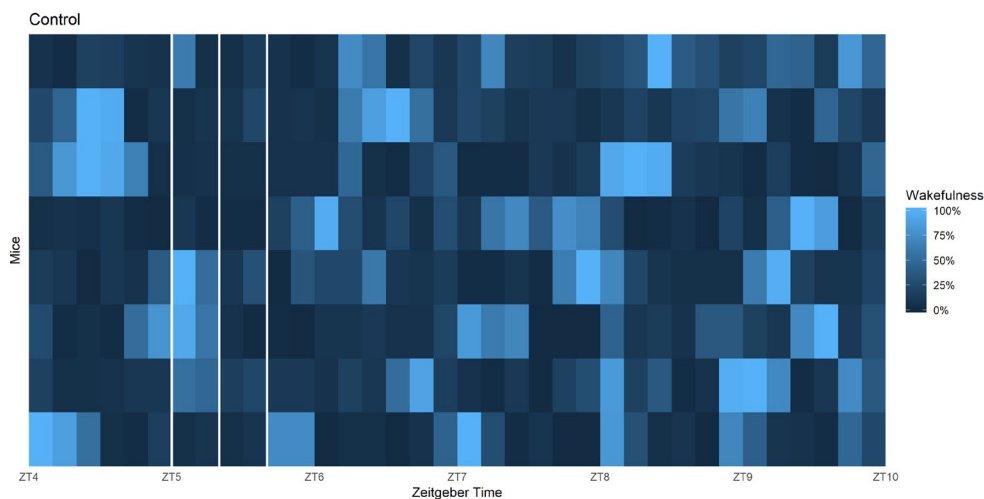


Figure 12: Heatmap of the proportion of wakefulness observed during, before and after stimulation in the control group ($n=4$). Each row represents one measurement, with the squares spanning 10-minute time bins. The fill color of squares represents the proportion of wakefulness within each 10-minute time bin and ranges from light blue (high proportion of wakefulness) to dark blue (low proportion of wakefulness). The x-axis gives Zeitgeber Time (ZT) measured as the number of hours after the lighting in home cages is turned on as an external cue (Zeitgeber). The white lines indicate the times of blue light exposure to the SCN.

Sleep stage proportions of individual mice and smoothed trend lines with 95% confidence intervals for wakefulness, REM and NREM sleep at baseline and during stimulation are plotted in figure 13. A side-to-side comparison of trajectories revealed a sharp onset of wakefulness in mice with SSFO expression in AVP neurons. The increase in wakefulness is simultaneously accompanied by a decrease in NREM sleep, while the proportion of REM sleep appeared to be unaffected (Figure 13). In summary, SSFO-mediated stimulation of AVP positive neurons in the SCN showed an increase in wakefulness with low latency that was observed in almost all experimental animals.

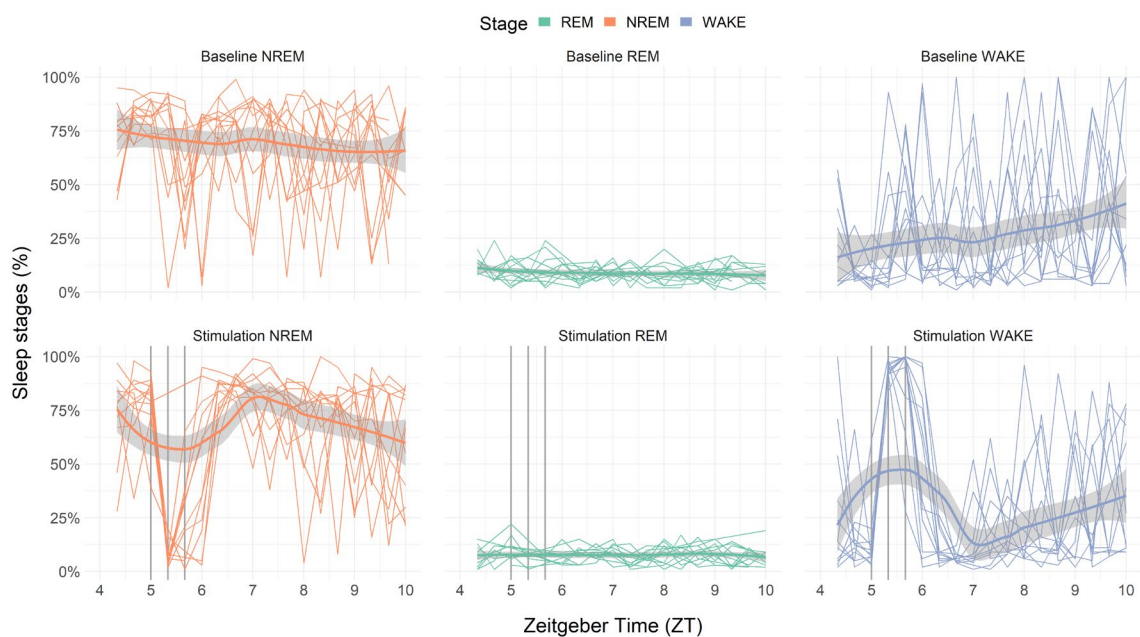


Figure 13: Sleep stage distributions at baseline and stimulation in 20-minute bins ($n=6$). Individual trajectories of measurements (two-fold per mouse) are given as thin lines, overlaid by smoothed trend lines with 95% confidence intervals from local polynomial regression fitting (LOESS). The two rows of panels represent baseline and stimulation conditions. The proportions of the three measured sleep stages are graphed separately in columns of the multi-panel figure. Additionally, the coloring of lines indicates the sleep stages: wakefulness (=WAKE, purple), non-rapid eye movement sleep (=NREM, red) and rapid eye movement sleep (=REM, green). The x-axis gives Zeitgeber Time (ZT) measured as the number of hours after the lighting in home cages is turned on as an external cue (Zeitgeber). The y-axis gives the proportion of sleep stages in percent (%).

Markov chain sleep stage transition analysis

To further investigate the increased proportion of wakefulness and the decreased proportion of NREM sleep, the transitions between sleep states were analyzed by modeling the sequence of sleep stages as a Markov process. Thus, a probability for the transition from one sleep stage to another was assigned for each point in time in the measurement period. A Markov chain phase transition analysis showed that mice expressing SSFO in AVP neurons showed a significant increase in the probability of awakening during the stimulation hour ($p = 0.023$). The transition probability between the stages NREM-WAKE, WAKE-WAKE and REM-WAKE was increased (Figure 14). A compensatory decrease in transitions to NREM and REM sleep could be observed. The transition probability between the stages WAKE-NREM, NREM-NREM, and REM-REM decreased (Figures 15 and 16). In the hour following the stimulation period, a sleep rebound was observed with an increase in the WAKE-NREM phase transitions (Figure 15) and a decrease in the WAKE-WAKE phase transition (Figure 14).

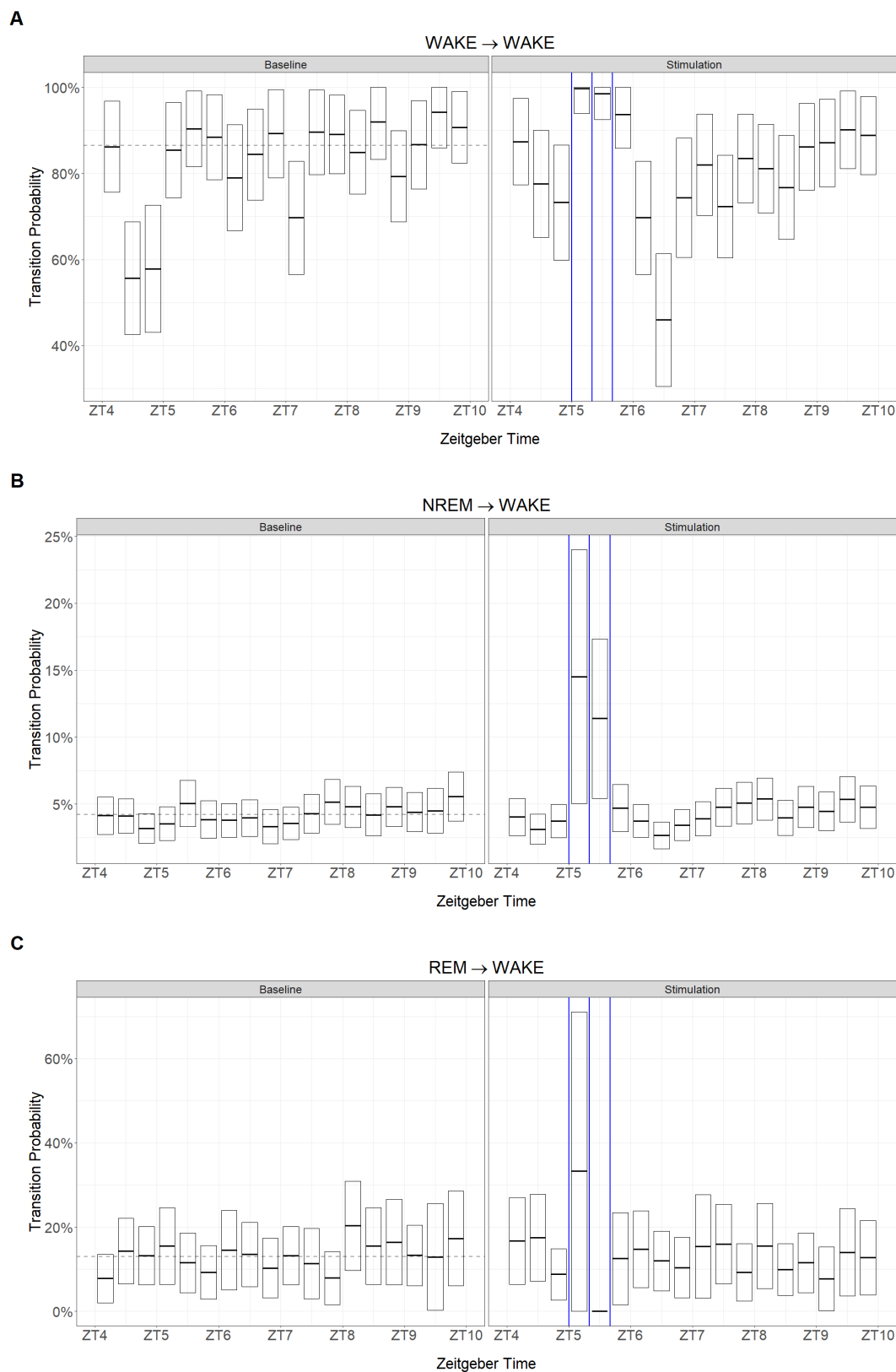


Figure 14: Sleep stage transition probabilities to wakefulness from WAKE (A), NREM (B) and REM (C). Probabilities are given in percent with a 95% confidence interval at baseline (left panel) and during stimulation (right panel). All probabilities were derived from the Markov chain model including measurements from mice with verified expression ($n=6$). For baseline measurements a transition probability for the whole period of observation is given as a horizontal dotted grey line. Blue vertical lines give the times of blue light stimulation.

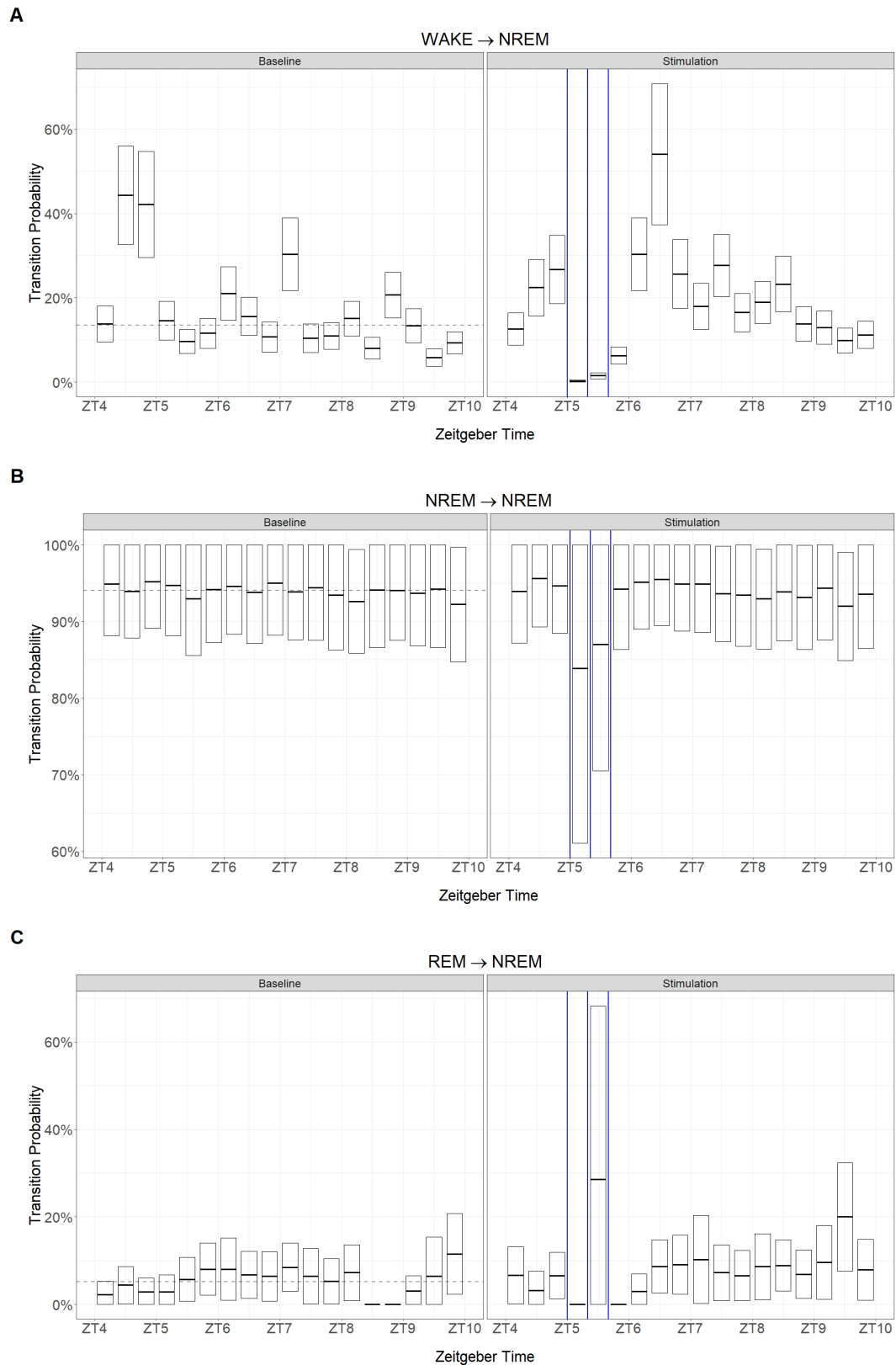


Figure 15: Sleep stage transition probabilities to NREM from WAKE (A), NREM (B) and REM (C). Probabilities are given in percent with a 95% confidence interval at baseline (left panel) and during stimulation (right panel). All probabilities were derived from the Markov chain model including measurements from mice with verified expression ($n=6$). For baseline measurements a transition probability for the whole period of observation is given as a horizontal dotted grey line. Blue vertical lines give the times of blue light stimulation.

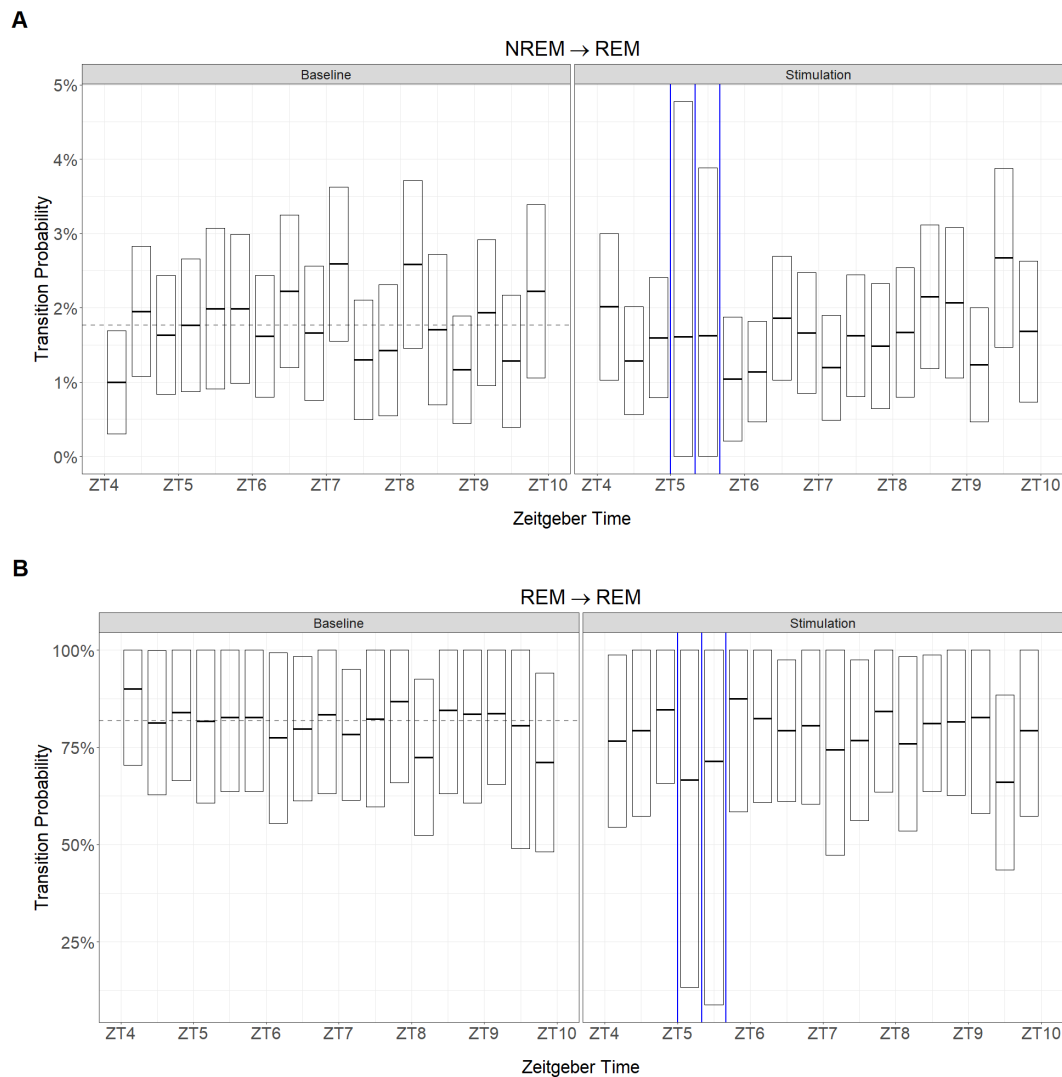


Figure 16: Sleep stage transition probabilities to REM from NREM (A) and REM (B). Probabilities are given in percent with a 95% confidence interval at baseline (left panel) and during stimulation (right panel). All probabilities were derived from the Markov chain model including measurements from mice with verified expression ($n=6$). For baseline measurements a transition probability for the whole period of observation is given as a horizontal dotted grey line. Blue vertical lines give the times of blue light stimulation. WAKE-REM sleep transition probability is not given since overall probability is zero and was not observed.

These effects were strongest at ZT 5. The effect at ZT 13 may be limited by the prerequisite that the animals were already mostly awake at this time point of their daily activity rhythm. In this analysis, only mice that showed SSFO expression in immunohistochemistry were included. The control group did not show such an effect during the hour of stimulation.

The transition probabilities between the time preceding stimulation (bin 1), stimulation (bin 4) and following stimulation (bin 7) were quantified and the data are given in Figure 17. Red arrows indicate a significant increase or decrease of transition probability between bin 1 and bin 4 or bin 1 and bin 7. Noticeably the probability of WAKE-WAKE in bin 4 was 1, which means that mice who were awake during that time were determined to stay awake. Compared to bin 1 this increase was significant ($p = 0.007$). Therefore, the probability of falling asleep (WAKE-NREM) was zero ($p < 0.001$). The probability of awakening (NREM-WAKE) increased from 0.04 in bin 1 to 0.15 in bin 4. This indicates that animals were significantly more likely to awaken from NREM sleep during stimulation ($p = 0.02$). In bin 7 the probability of WAKE-WAKE was 0.7 and WAKE-NREM was 0.3. Compared to bin 1 the probability of mice staying awake was significantly decreased ($p = 0.004$), while the probability of falling asleep was significantly increased ($p < 0.001$). All other transition probabilities were not significantly different from bin 1. Therefore, the Markov chain sleep stage analysis showed that SSFO-mediated stimulation significantly increases wakefulness and is followed by a significant decrease in wakefulness thereafter.

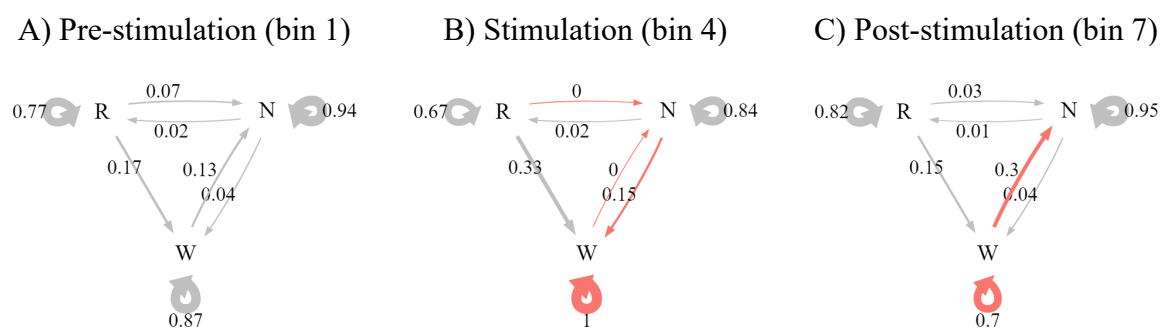


Figure 17: Transition probabilities ($n=6$) at time bins 1 hour before stimulation (A), during stimulation (B) and 1 hour after stimulation (C), which correspond to ZT4:00-ZT4:20, ZT5:00-ZT5:20 and ZT6:00-ZT6:20. Stages were labeled “R”, “N” and “W” for REM, NREM and WAKE. Arrow width corresponds to transition probability, which is additionally added as a label for each arrow. For panel B and C pairwise comparison of transition probabilities to panel A were performed with Welch’s *t*-test. Arrows with significant increase or decrease ($p < 0.05$) were colored red. P-values for panel B are $W \rightarrow W$ 0.0073, $W \rightarrow N$ 0.00015, $N \rightarrow W$ 0.023 and $R \rightarrow N$ 0.036. P-values for panel C are $W \rightarrow W$ 0.0043 and $W \rightarrow N$ 0.00039.

Electrophysiological function of stabilized step function opsin in AVP neurons

To characterize the effect of SSFO activation in AVP neurons, whole cell voltage-clamp and current-clamp techniques were used in acute SCN slices. This provided further evidence for the successful and functional expression of the opsin in AVP neurons. Voltage clamp recordings of an AVP neuron expressing SSFO in acute SCN slices showed an inward photocurrent triggered by illumination with blue light. Peak photocurrents were measured at -251 pA. This corresponds to the active state of SSFO. The flashing of orange light returned the membrane potential to baseline (Figure 18).

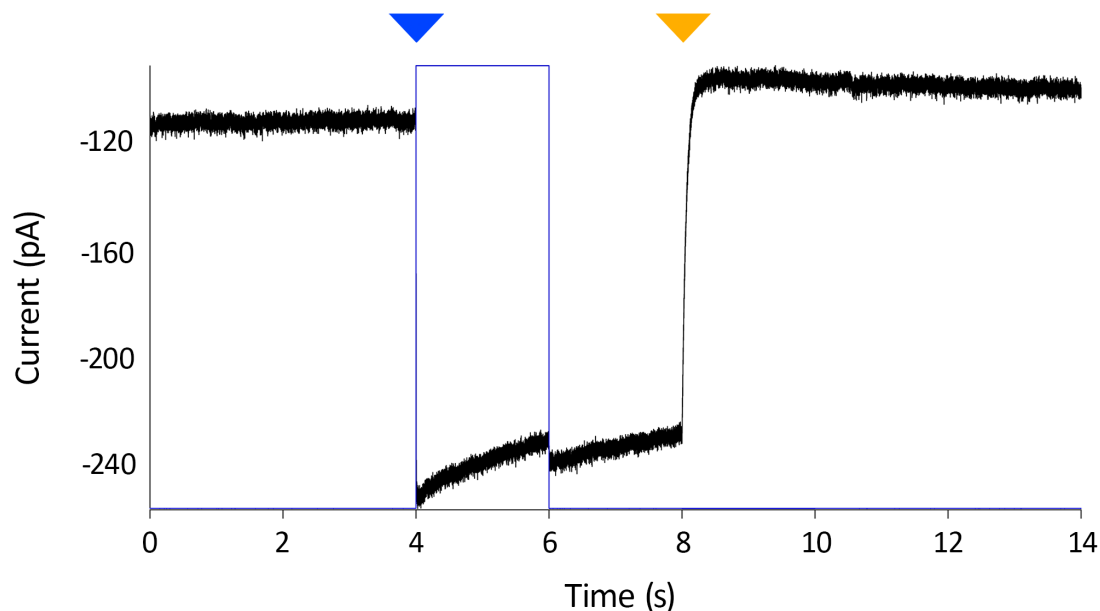


Figure 18: AVP neurons voltage clamp of optogenetic activation and inactivation. Blue arrowhead indicates onset of 2s of blue light (473 nm). Orange arrowhead indicates onset of 2s of orange light (561 nm). X-axis given in seconds and y-axis in pA.

Under current clamp conditions, the two-second blue-light flash evoked one action potential followed by a continuous depolarization of the cell membrane by +20 mV from baseline. I theorized that the blue light-induced opening of SSFO in the cell membrane caused a slight depolarization through the influx of cations. This in turn opened voltage-gated sodium channels that caused the observed action potential. Afterward, the continuous

depolarization inhibited the reactivation of voltage-gated sodium channels. The hyperpolarization required to overcome the refractory state of these channels was omitted. Cells that were found to be spiking at baseline, ceased to spike after flashing of blue light (Figure 19). Together, these results show that AVP neurons expressing SSFO can be electrically controlled with light.

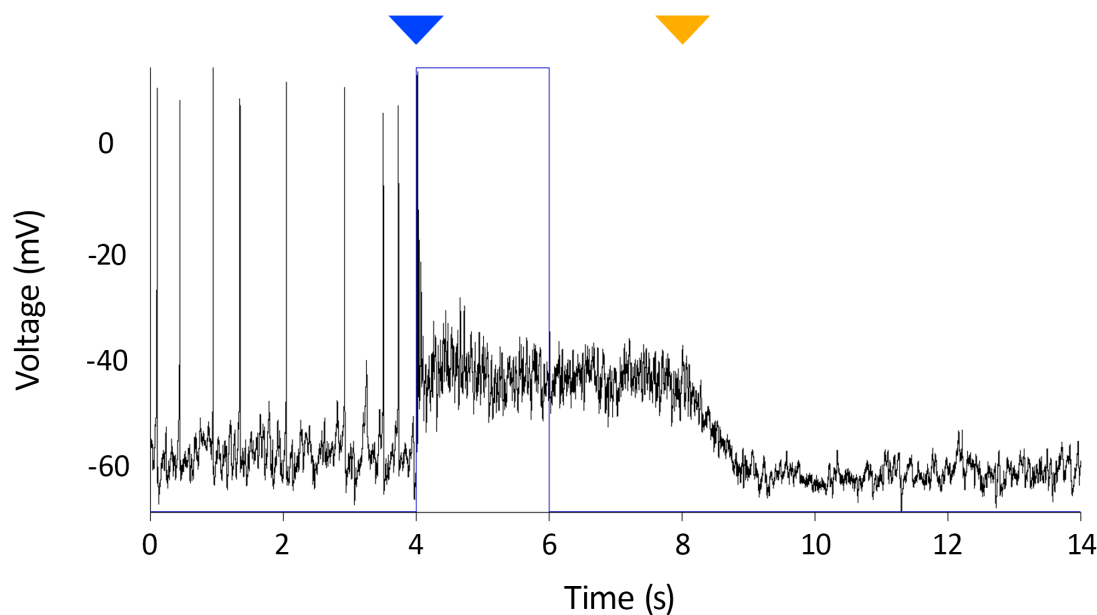


Figure 19: AVP neuron current clamp of optogenetic activation and inactivation. Blue arrowhead indicates onset of 2s of blue light (473 nm). Orange arrowhead indicates onset of 2s of orange light (561 nm). X-Axis given in seconds and y-axis in mV.

Furthermore, when continuously measuring in current clamp mode for 20 minutes, a depolarization initiated after 3 minutes of baseline recording showed a distinct long-lasting effect on AVP neurons. Originally from a rather shallow -60 mV membrane potential, an initial action potential upon blue light was followed by a continuous depolarized membrane state of -40 mV, slowly returning to -60 mV over the course of over 17 minutes. This highlights the activation kinetics of SSFO with a long-lasting active state (Figure 20). In summary, the electrophysiological experiments indicate the functional expression of SSFO with a long-lasting effect on the electrical activity of AVP neurons.

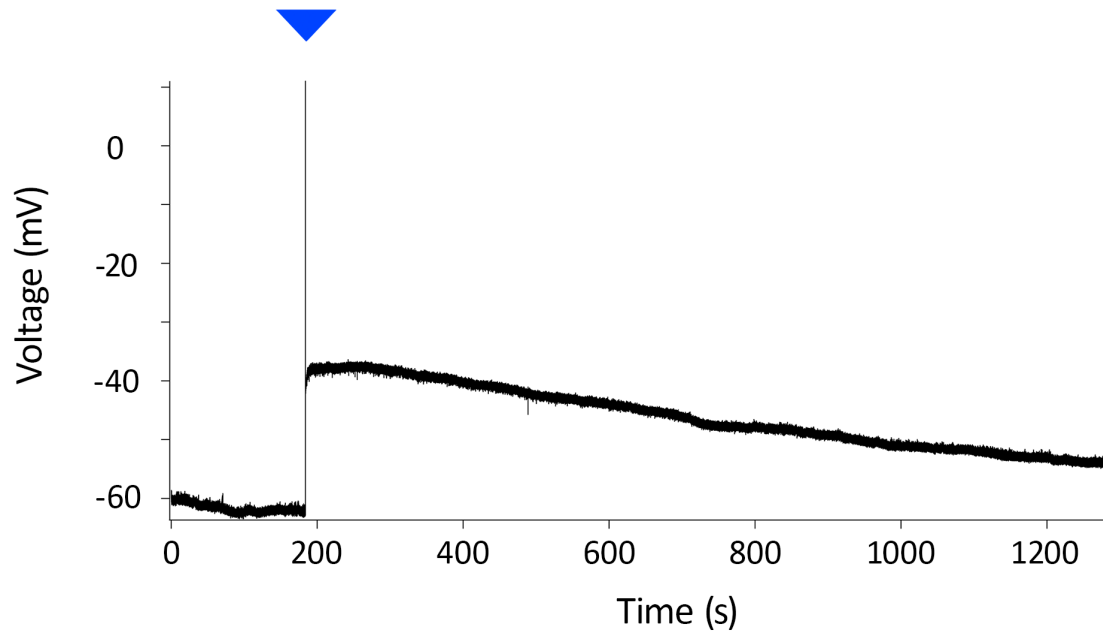


Figure 20: AVP neuron current clamp 20-minute continuous measurement after SSFO-mediated depolarization. Blue arrowhead indicates onset of 2s of blue light (473 nm). X-Axis given in seconds and y-axis in mV.

Discussion

For this thesis, I present a possible connection between the central circadian clock and sleep behavior in mammals. SSFO-mediated stimulation of AVP positive neurons in the SCN increased the total amount of wakefulness during the hour of stimulation. Interestingly, this effect led to a rebound in sleep in the hour after the stimulations. A Markov chain sleep stage analysis showed that optogenetic stimulation had an immediate effect on sleep stage transition probabilities. Most significantly, the probabilities of transition to wakefulness increased compared to the hour before stimulation. After the end of stimulation, transition probabilities to wakefulness were significantly decreased. This suggests that any form of sleep deprivation is followed by a compensatory increase in the time spent sleeping in the following period. The observed recovery to baseline was rather quick and one hour after the end of stimulation there was no observable effect. *Ex vivo*, SSFO activation in AVP neurons caused depolarizations that resulted in the potential prolonged silencing and cessation of action potential firing in SCN slices.

Only two other research groups have previously demonstrated the effect of direct optogenetic stimulation of the SCN *in vivo* on circadian behaviors. The first study aimed to express ChR2 under a less specific driver directed at the SCN (dopamine receptor D1a) and thus expression was not limited to AVP neurons (Jones et al. 2015). Expression was reported to be ~90% in both AVP and VIP neurons throughout the SCN. Furthermore, mice were kept under constant darkness and thereby allowed to free run while tracking locomotor activity. Using this experimental setup, they were able to show a progressive alignment of the onset of activity with the timing of optogenetic stimulation of the SCN in free-running mice. They concluded a downstream effect on locomotor behavior by optogenetically stimulating the SCN. This was confirmed in this study and further narrowed down to AVP neurons. Without other external cues an arousing effect caused by direct stimulation of AVP neurons could

explain a phase shifting effect as reported by Jones, Tackenberg et al. study in 2015. In a follow-up study the same group was able to further narrow down the effect of optogenetic stimulation of VIP neurons as a shortening of the SCN free-running period (Tackenberg et al. 2021).

A second research group used chronic optogenetic stimulation of the SCN to elucidate a possible connection with depression and/or anxiety (Vadnie et al. 2021). In this case, ChR2 was expressed under a SCN-directed driver (*Vgat*) and was also not limited to AVP neurons. Because this study focused more on psychiatric-related behaviors in mice, behavioral assessments (e.g., open field, elevated plus maze, forced swim test) were conducted in addition to locomotor activity assessment. They were able to demonstrate an increase in anxiety-related behavior after optogenetic stimulation of the SCN. Anxiety-related behavior triggered by optogenetic stimulation of the SCN can be interpreted as a correlate of the arousal effect observed in this thesis. Under this assumption, Vadnie et al. 2021 supports the effect presented here. This combination of findings provides some support for the idea that arousal emanating from the mammalian circadian pacemaker may influence anxiety-related behavior. Such a pathway could provide a conceptual basis for the association between disrupted circadian rhythms and psychiatric disorders that has been shown in humans (Vadnie and McClung 2017, Logan and McClung 2019).

In this thesis, the optogenetically induced arousal could be triggered in a temporal precise and repetitive manner. Three consecutive stimulations with 20-minute intervals in between always promoted wakefulness. The extent of the effect was exhaustible and was already visibly diminished by the third successive repetition. Although many brain nuclei are involved in the transition from sleep to wakefulness, only a limited number of areas have been shown to induce wakefulness or even insomnia upon optogenetic stimulation. In particular, other brain regions very close to or directly connected to the SCN have been

identified as promoting wakefulness. Orexin neurons in the lateral hypothalamic area (LHA) are known to play a critical role in mediating arousal and linking arousal to energy balance, emotions, and the reward system (Sakurai 2007). Neurodegeneration of these neurons has been identified as a probable main cause of narcolepsy in humans (Peyron et al. 2000, Thannickal et al. 2000). Later optogenetic studies showed that activation of orexin neurons causes a rapid shift from NREM sleep or REM sleep to wakefulness (Adamantidis et al. 2007) and that inhibition of orexin neurons induces NREM sleep (Tsunematsu et al. 2011). This further confirmed the causality between orexin neurons and sleep states. The effect observed by optogenetic activation of orexin neurons is strikingly similar to the effect presented in this thesis in terms of the latency and kinetics of state transitions. The similarity goes to the extent that indeed a link between the two effects could be postulated.

Immunohistochemical studies have established neuronal fibers between the LHA and the SCN (Peyron et al. 1998, Cutler et al. 1999, McGranaghan and Piggins 2001). Furthermore, direct interaction between the SCN and orexin neurons in the tuberal hypothalamus has been suggested in a previous study (Marston et al. 2008). This combination of findings suggests that orexin neurons are a potential downstream effector of AVP neurons and together form a larger neural circuit that regulates sleep-wake behavior. More studies will be required to investigate the connection between AVP neurons and orexin neurons. Characterization of a link between the SCN and orexin neurons in the LHA may also be of clinical importance, as the effect of pharmacological antagonism in the orexin system has already been translated to humans (Brisbare-Roch et al. 2007) and could have potential to be extended to diseases with circadian disruption.

Another potential effector that could explain the observed facilitation of wakefulness is the preoptic area. While the preoptic area contains mainly sleep-promoting neurons, reduced activation of this neuronal target could lead to increased wakefulness. The prolonged

depolarization observed in the electrophysiological experiments with possible cessation of action potential firing could be considered as neuronal silencing. In this context, a general reduction in downstream target activation could be considered as the main effect of SSFO activation in AVP neurons. Neuroanatomical studies in 2002 and 2005 by Deurveilher et al. indicate neuronal projections from the shell of the SCN via the medial preoptic area, the subparaventricular zone, and the dorsomedial hypothalamic nucleus to sleep-promoting neurons in the preoptic area (Deurveilher et al. 2002, Deurveilher and Semba 2005). A reduced activation of this circuit might explain a direct wakefulness-promoting effect from the SSFO stimulation of AVP neurons. If silencing of AVP neurons promotes wakefulness, this may indicate their role as initiators of sleep behavior in the circadian rhythm of mice. Further studies should validate these results and identify downstream targets for AVP-neurons. It remains also critical to differentiate the arousal effect from other AVP neurons outside of the SCN.

Recent studies proposed another neuronal pathway originating in the SCN that is involved in the regulation of sleep and wakefulness (Li et al. 2020, Ono et al. 2020). Through optogenetic stimulation of CRH neurons in the PVH, they demonstrated increased wakefulness, while chemogenetic inhibition resulted in increased NREM sleep. They also showed that this effect was at least partially mediated by the activation of orexin neurons in the LHA. These results provide a foundation to clarify the mechanisms underlying stress-induced insomnia. Finally, these studies found that GABAergic neurons in the SCN could regulate the neuronal activity of CRH neurons in the PVN. While GABAergic neurons have not been described as a well-defined subpopulation of SCN neurons (Wen et al. 2020), GABA is known to colocalize significantly with AVP among other neurotransmitters in the SCN (Moore and Speh 1993, Buijs et al. 1995, Abrahamson and Moore 2001). This could place AVP neurons, as described in this thesis, in a strategic position to orchestrate sleep and

arousal behaviors. Furthermore, it is highly likely that there is a functional pathway that controls the regulation of wakefulness by the mammalian circadian pacemaker.

The present study not only showed that SSFO stimulation of AVP neurons modulates arousal state transitions, but also causes a total increase in wakefulness during the hour of stimulation. This contrasts with most other studies that promoted wakefulness. Shorter photostimulation studies (1-30 min) have described a longer duration of episodes of wakefulness during stimulation (Kodani et al. 2017). Although chronic photostimulation protocols over similar extends of time (1h) (Adamantidis et al. 2007) have shown an increased state transition probability to wakefulness, they concluded no increase in total wake during the observation period. This could indicate that the magnitude of arousal observed in this thesis could be stronger than previous studies were able to demonstrate. Similar orders of magnitude have previously only been described in extensive photostimulation (6h) studies of neurons directly targeting the LHA (Li et al. 2020). Another common strategy for applying optogenetic stimulation is to set triggers in real-time EEG/EMG analysis. With this strategy, stimulation can be conditioned to stable states of sleep phases (e.g., 15s after the onset of stable REM sleep) (Carter et al. 2009). Thereby, the experimental effects on specific sleep stages and wake-up latency can be better examined. This strategy was not applied in the study described here, as it was focused on chronic stimulation of neurons in the SCN. To my knowledge, no study has previously reported a compensatory increase in NREM sleep after periods of prolonged optogenetically induced wakefulness. This may suggest that optogenetic stimulation-induced wakefulness could be considered as sleep deprivation. The effects of sleep deprivation on sleep stages have been well studied, and in particular, a compensatory increase in NREM sleep after sleep deprivation has been well described in both rodents and humans (Borbély and Neuhaus 1979, Brunner et al. 1990).

The state of wakefulness could also be facilitated at different Zeitgeber times, but the extent of the acute effect was time-of-day dependent. Increased sleep pressure has been shown to modulate the effect of promoting wakefulness with optogenetics in sleep deprivation studies (Carter et al. 2009). SSFO stimulation of AVP neurons was successfully tested at ZT5 and ZT13. These times closely resemble what other studies have determined to be optimal conditions for influencing sleep-wake behavior, as sleep pressure does not appear to be too great and wakefulness can be adequately studied (Tsunematsu et al. 2011, Jones et al. 2015, Zant et al. 2016, Kodani et al. 2017, Ono et al. 2020). At ZT 13, the proportion of induced wakefulness was noticeably lower. This could be explained by the fact that mice already spent most of their time awake at that time in their circadian cycle. Therefore, the increase in wakefulness from baseline measured at ZT13 after activation of SSFO was rather small. When we repeated the experiments for all mice, mice that responded with a promotion of wakefulness upon activation of SSFO before always showed a similarly strong effect in the subsequent experiments. A twofold repetition of optogenetic experiments for each mouse seems to be common among optogenetic studies (Adamantidis et al. 2007). Therefore, I assumed that brain structure and integrity were not altered further after implantation of the electrodes and optical fiber and that stimulation of AVP neurons by SSFO itself is unlikely to have an altering effect on brain structure and function.

The electrophysiological experiments were designed to examine the influence of SSFO on AVP neurons. As mentioned in the introduction, there are few reports on the effect of prolonged SSFO activation (Berndt et al. 2009, Jégo et al. 2013). I hypothesize that SSFO activation causes a quick action potential in AVP neurons which is followed by a continuous depolarization. One other study has found that optogenetic activation of SSFO in GABAergic neurons in SCN slices increases Ca^{2+} levels (Ono et al. 2020). This could indicate that SCN neurons are initially activated by photostimulation. In other contexts, it has been

hypothesized that neurons show increased excitability after activation of SSFO (Berndt et al. 2009, Jegu et al. 2013). I found that prolonged activation of SSFO in AVP neurons caused mild depolarization and potential silencing of action potential firing in SCN slices. This is explained by a continuous open state of the light-sensitive ion channel upon photoactivation, permitting a continuous influx of cations. This approach of optogenetic stimulation in the SCN contrasts with other studies (Jones et al. 2015, Vadnie et al. 2021) that examined the SCN with optogenetic constructs using mainly ChR2, which showed increased neuronal firing upon stimulation. For this study, I also experimented with ChR2 but found bigger effect sizes with SSFO.

Getting a consistent quality of electrophysiological recordings proved to be a very challenging task. Cells found to be positive for AVP responded very heterogeneously in their spiking behavior and resting membrane potential. I used a cocktail of receptor blockers to isolate the AVP neurons from the network. Still their neural activity in my recordings had a high heterogeneity. Further heterogeneity within the targeted population of AVP neurons, and thus its response to mild depolarization may explain these findings. Recently, for example, five neuron subtypes in the SCN with heterogeneous circadian gene expression have been described (Wen et al. 2020). Although the electrophysiological experiments gave an indication of how activation of SSFO affects AVP neurons, in general only a few successful and high-quality recordings were obtained. Other analysis and quantitative evaluations were unfortunately not possible. Therefore, this part of the study is inconclusive, and only a very general idea of the electrophysiological effect of SSFO in AVP neurons can be derived.

Overall, the experimental setup is comparable to other studies and the protocols are very similar to other standard works in the literature (Adamantidis et al. 2007, Jones et al. 2021). The optogenetic stimulation procedures were designed to mimic the effects of environmental light on the SCN and were based on previously described optogenetic

stimulation paradigms (Jones et al. 2015, Vadnie et al. 2021). The group size for the main part of the experiments ranged between 6 and 9 animals, which is comparable to other studies in this field (Adamantidis et al. 2007, Carter et al. 2009).

The effects reported in this thesis already occurred with unilateral stimulation, suggesting that AVP neurons play a strong and causal role in driving awakening. These results are consistent with other studies that have shown that unilateral optogenetic manipulation of neurons (e.g., Orexin or CRH neurons) is sufficient to promote wakefulness (Adamantidis et al. 2007, Carter et al. 2009, Li et al. 2020). Bilateral optogenetic stimulation can have an even stronger effect on promoting and maintaining wakefulness and has been reported for some optogenetic studies (Tsunematsu et al. 2011).

Repeated measurements in each mouse with a resting interval of at least 72 hours showed that the observed effect was reproducible and could correspond to an underlying neural circuit. This repetition interval is very similar to other optogenetic studies in this field and is mainly followed to eliminate a confounding effect from one stimulation interval to another stimulation interval (Carter et al. 2009, Tsunematsu et al. 2011, Vadnie et al. 2021). Furthermore, this repetition interval of experiments controls to some extent the influence of any infradian rhythms in the promotion of wakefulness (Eastwood et al. 1985, Wollnik 1989).

Mice that received the implants did not show secondary effects or impairments. They behaved normally and adapted well to the experimental setup. In mice with intense postsurgical pain or anxiety-related behavior, this should be visibly altered. Only in four cases complications occurred. Three of them were cases in which mice did not wake up again from surgery. This might be due to over-dosing of anesthetics or traumatic injury during the procedure. In the fourth case, a mouse developed significant weight loss and signs of infection in the week after surgery and was then sacrificed. All other mice fully healed after surgery and underwent the entire set of measurements without problems.

The three main sources of confounding arousal in mice were identified as discomfort, light, and equipment. A control group was included to exclude other such arousal effects. Specifically, these issues arise in the following form: mice were continuously tethered to an optogenetic fiber and EEG/EMG electrodes that can lead to tangling, restriction of movement, and discomfort. In terms of light leakage, the optogenetic devices and the measures taken have largely limited light leakage. However, at the junction between the implant and the tethered optic fiber, it is difficult to fully avoid them. I controlled both issues by stimulating experimental and control mice identically. In the control group, optogenetic stimulation did not show an effect on the frequency of sleep stages or the probabilities of transition. Since control and experimental groups were treated under the exact same conditions and protocols, any other wakefulness-inducing effects by the experiments can be ruled out. I also completely removed the experimenter from the setting during the stimulation times by connecting the mice to the electrodes and optical fiber at least one hour before the start of the recording and triggering the laser with a minicomputer. This should eliminate any arousing effects by the presence of human beings during the experiments (Wollnik 1989, Chesler et al. 2002).

However, based on the used optogenetic technique, ectopic stimulation cannot be ruled out as a factor for the observed effects. Expression of the optogenetic construct might be strictly limited to neurons that express AVP, but AVP neurons are not exclusively found in the SCN. In particular, expression of SSFO was observed in the thalamic reticular nucleus, the thalamic paraventricular nucleus, the hypothalamic paraventricular nucleus and the supraoptic nucleus for some mice. As Mieda et al. 2015 has shown before this expression of AVP in neurons outside the SCN is limited. In two mice, the arousal effect was observed upon SSFO stimulation without detectable expression in AVP neurons of the SCN. In these two mice, the expression of SSFO was limited to the reticular and paraventricular thalamic

nuclei. The immunohistology confirmed that the optical fiber targets only medial structures and even bypasses the thalamic regions in most sections. Therefore, light exposure to the thalamic nuclei, and especially the reticular thalamic nucleus, and the ensuing activation of SSFO there should be minimal. It remains inconclusive to differentiate the arousal effect from other neuronal regions, but the results presented in this thesis indicate that AVP neurons have a direct downstream influence on sleep behavior.

Acknowledgements

I became a scientist because of my mother, Petra Rumpf, who taught me endless curiosity and a hands-on mentality. In her life and work, she expressed full dedication and commitment. She was also the first member of my family to pursue an academic career and obtain a Ph.D. My father, Johannes Rumpf, sparked my interest in medicine and patient care. He embodies the qualities of a good doctor: empathy, humility, perseverance, and the ability to really listen to people. I do not always meet the exact standard of care that he sets for himself in his medical work, but I came to understand why it is the right standard. To escape their influence, I would have had to be blind and deaf.

The research on which this thesis is based was originally conceived in 2017 as an exchange project between the University of Kanazawa, Japan, and the University of Wuerzburg, Germany. This would not have been possible without effective supervisors who were always readily available to provide guidance for such a particular project. I foremost thank my thesis supervisors Charlotte Helfrich-Förster, Carmen Villmann, and Michihiro Mieda. I also thank Robert Johannes Kittel, who helped me get this project off the ground before anyone else believed it would work.

Most of the work I did would not have been possible without the assistance and instruction I received from other great researchers: Dirk Rieger, Takashi Maejima, Yusuke Tsuno, Ayako Matsui, Fukushi, Masumi Kawabata.

I greatly benefited from the comments and discussion with a number of people on earlier drafts of this manuscript: Christina Albrecht, Trese Leinders-Zufall, Roman Hauber and Leon Harrer.

I am grateful to Esther Duflo who sparked my interest in statistics and data science during a lecture at MIT that I was lucky to hear in 2018. She gave great inspiration for conducting meaningful research and writing acknowledgements.

Bibliography

Abrahamson, E. E. and R. Y. Moore (2001). Suprachiasmatic nucleus in the mouse: retinal innervation, intrinsic organization and efferent projections. Brain Research **916**(1): 172-191.

Adamantidis, A. R., F. Zhang, A. M. Aravanis, K. Deisseroth and L. de Lecea (2007). Neural substrates of awakening probed with optogenetic control of hypocretin neurons. Nature **450**(7168): 420-424.

Allen, C. N., M. N. Nitabach and C. S. Colwell (2017). Membrane Currents, Gene Expression, and Circadian Clocks. Cold Spring Harb Perspect Biol **9**(5).

Anaclet, C., L. Ferrari, E. Arrigoni, C. E. Bass, C. B. Saper, J. Lu and P. M. Fuller (2014). The GABAergic parafacial zone is a medullary slow wave sleep-promoting center. Nature Neuroscience **17**(9): 1217-1224.

Atkinson, S. E., E. S. Maywood, J. E. Chesham, C. Wozny, C. S. Colwell, M. H. Hastings and S. R. Williams (2011). Cyclic AMP signaling control of action potential firing rate and molecular circadian pacemaking in the suprachiasmatic nucleus. J Biol Rhythms **26**(3): 210-220.

Balsalobre, A., F. Damiola and U. Schibler (1998). A serum shock induces circadian gene expression in mammalian tissue culture cells. Cell **93**(6): 929-937.

Berndt, A., O. Yizhar, L. A. Gunaydin, P. Hegemann and K. Deisseroth (2009). Bi-stable neural state switches. Nature Neuroscience **12**(2): 229-234.

Borbély, A. A. and H. U. Neuhaus (1979). Sleep-deprivation: Effects on sleep and EEG in the rat. Journal of comparative physiology **133**(1): 71-87.

Brancaccio, M., E. S. Maywood, J. E. Chesham, A. S. Loudon and M. H. Hastings (2013). A Gq-Ca²⁺ axis controls circuit-level encoding of circadian time in the suprachiasmatic nucleus. Neuron **78**(4): 714-728.

Brisbare-Roch, C., J. Dingemans, R. Koberstein, P. Hoeber, H. Aissaoui, S. Flores, C. Mueller, O. Nayler, J. van Gerven, S. L. de Haas, P. Hess, C. Qiu, S. Buchmann, M. Scherz, T. Weller, W. Fischli, M. Clozel and F. Jenck (2007). Promotion of sleep by targeting the orexin system in rats, dogs and humans. Nat Med **13**(2): 150-155.

Brunner, D. P., D. J. Dijk, I. Tobler and A. A. Borbély (1990). Effect of partial sleep deprivation on sleep stages and EEG power spectra: evidence for non-REM and REM sleep homeostasis. Electroencephalogr Clin Neurophysiol **75**(6): 492-499.

Buijs, R. M., J. Wortel and Y.-X. Hou (1995). Colocalization of γ -aminobutyric acid with vasopressin, vasoactive intestinal peptide, and somatostatin in the rat suprachiasmatic nucleus. Journal of Comparative Neurology **358**(3): 343-352.

Carter, M. E., A. Adamantidis, H. Ohtsu, K. Deisseroth and L. de Lecea (2009). Sleep Homeostasis Modulates Hypocretin-Mediated Sleep-to-Wake Transitions. The Journal of Neuroscience **29**(35): 10939-10949.

Chen, K. S., M. Xu, Z. Zhang, W. C. Chang, T. Gaj, D. V. Schaffer and Y. Dan (2018). A Hypothalamic Switch for REM and Non-REM Sleep. Neuron **97**(5): 1168-1176.e1164.

Chesler, E. J., S. G. Wilson, W. R. Lariviere, S. L. Rodriguez-Zas and J. S. Mogil (2002). Influences of laboratory environment on behavior. Nature Neuroscience **5**(11): 1101-1102.

Chung, S., F. Weber, P. Zhong, C. L. Tan, T. N. Nguyen, K. T. Beier, N. Hörmann, W. C. Chang, Z. Zhang, J. P. Do, S. Yao, M. J. Krashes, B. Tasic, A. Cetin, H. Zeng, Z. A. Knight,

L. Luo and Y. Dan (2017). Identification of preoptic sleep neurons using retrograde labelling and gene profiling. Nature **545**(7655): 477-481.

Cuesta, M., D. Clesse, P. Pevet and E. Challet (2009). From daily behavior to hormonal and neurotransmitters rhythms: comparison between diurnal and nocturnal rat species. Horm Behav **55**(2): 338-347.

Cutler, D. J., R. Morris, V. Sheridhar, T. A. Wattam, S. Holmes, S. Patel, J. R. Arch, S. Wilson, R. E. Buckingham, M. L. Evans, R. A. Leslie and G. Williams (1999). Differential distribution of orexin-A and orexin-B immunoreactivity in the rat brain and spinal cord. Peptides **20**(12): 1455-1470.

Deboer, T., L. Detari and J. H. Meijer (2007). Long term effects of sleep deprivation on the mammalian circadian pacemaker. Sleep **30**(3): 257-262.

Debruyne, J. P., E. Noton, C. M. Lambert, E. S. Maywood, D. R. Weaver and S. M. Reppert (2006). A clock shock: mouse CLOCK is not required for circadian oscillator function. Neuron **50**(3): 465-477.

Deurveilher, S., J. Burns and K. Semba (2002). Indirect projections from the suprachiasmatic nucleus to the ventrolateral preoptic nucleus: a dual tract-tracing study in rat. Eur J Neurosci **16**(7): 1195-1213.

Deurveilher, S. and K. Semba (2005). Indirect projections from the suprachiasmatic nucleus to major arousal-promoting cell groups in rat: implications for the circadian control of behavioural state. Neuroscience **130**(1): 165-183.

Eastwood, M. R., J. L. Whitton, P. M. Kramer and A. M. Peter (1985). Infradian Rhythms: A Comparison of Affective Disorders and Normal Persons. Archives of General Psychiatry **42**(3): 295-299.

Edgar, D. M., W. C. Dement and C. A. Fuller (1993). Effect of SCN lesions on sleep in squirrel monkeys: evidence for opponent processes in sleep-wake regulation. J Neurosci **13**(3): 1065-1079.

Enoki, R., S. Kuroda, D. Ono, M. T. Hasan, T. Ueda, S. Honma and K. Honma (2012). Topological specificity and hierarchical network of the circadian calcium rhythm in the suprachiasmatic nucleus. Proc Natl Acad Sci U S A **109**(52): 21498-21503.

Enoki, R., Y. Oda, M. Mieda, D. Ono, S. Honma and K. I. Honma (2017). Synchronous circadian voltage rhythms with asynchronous calcium rhythms in the suprachiasmatic nucleus. Proc Natl Acad Sci U S A **114**(12): E2476-E2485.

Helfrich-Forster, C. (1998). Robust circadian rhythmicity of *Drosophila melanogaster* requires the presence of lateral neurons: a brain-behavioral study of disconnected mutants. J Comp Physiol A **182**(4): 435-453.

Herdegen, T. and J. D. Leah (1998). Inducible and constitutive transcription factors in the mammalian nervous system: control of gene expression by Jun, Fos and Krox, and CREB/ATF proteins. Brain Res Brain Res Rev **28**(3): 370-490.

Herzog, E. D., T. Hermansteyne, N. J. Smyllie and M. H. Hastings (2017). Regulating the Suprachiasmatic Nucleus (SCN) Circadian Clockwork: Interplay between Cell-Autonomous and Circuit-Level Mechanisms. Cold Spring Harb Perspect Biol **9**(1): a027706.

Huang, R.-C. (2018). The discoveries of molecular mechanisms for the circadian rhythm: The 2017 Nobel Prize in Physiology or Medicine. Biomedical Journal **41**(1): 5-8.

Inouye, S. T. and H. Kawamura (1979). Persistence of circadian rhythmicity in a mammalian hypothalamic "island" containing the suprachiasmatic nucleus. Proceedings of the National Academy of Sciences **76**(11): 5962-5966.

Jego, S., S. D. Glasgow, C. G. Herrera, M. Ekstrand, S. J. Reed, R. Boyce, J. Friedman, D. Burdakov and A. R. Adamantidis (2013). Optogenetic identification of a rapid eye movement sleep modulatory circuit in the hypothalamus. Nature Neuroscience **16**(11): 1637-1643.

Jones, J. R., M. C. Tackenberg and D. G. McMahon (2015). Manipulating circadian clock neuron firing rate resets molecular circadian rhythms and behavior. Nat Neurosci **18**(3): 373-375.

Jones, J. R., M. C. Tackenberg and D. G. McMahon (2021). Optogenetic Methods for the Study of Circadian Rhythms. Circadian Clocks: Methods and Protocols. S. A. Brown. New York, NY, Springer US: 325-336.

Kodani, S., S. Soya and T. Sakurai (2017). Excitation of GABAergic Neurons in the Bed Nucleus of the Stria Terminalis Triggers Immediate Transition from Non-Rapid Eye Movement Sleep to Wakefulness in Mice. The Journal of Neuroscience **37**(30): 7164-7176.

Lee, I. T., A. S. Chang, M. Manandhar, Y. Shan, J. Fan, M. Izumo, Y. Ikeda, T. Motoike, S. Dixon, J. E. Seinfeld, J. S. Takahashi and M. Yanagisawa (2015). Neuromedin s-producing neurons act as essential pacemakers in the suprachiasmatic nucleus to couple clock neurons and dictate circadian rhythms. Neuron **85**(5): 1086-1102.

Li, S.-B., J. C. Borniger, H. Yamaguchi, J. Hédou, B. Gaudilliere and L. de Lecea (2020).

Hypothalamic circuitry underlying stress-induced insomnia and peripheral

immunosuppression. Science Advances **6**(37): eabc2590.

Liang, X., T. E. Holy and P. H. Taghert (2016). Synchronous *Drosophila* circadian

pacemakers display nonsynchronous Ca²⁺ rhythms in vivo. Science **351**(6276): 976-981.

Liang, X., T. E. Holy and P. H. Taghert (2017). A Series of Suppressive Signals within the

Drosophila Circadian Neural Circuit Generates Sequential Daily Outputs. Neuron **94**(6):

1173-1189.e1174.

Logan, R. W. and C. A. McClung (2019). Rhythms of life: circadian disruption and brain

disorders across the lifespan. Nat Rev Neurosci **20**(1): 49-65.

Marston, O. J., R. H. Williams, M. M. Canal, R. E. Samuels, N. Upton and H. D. Piggins

(2008). Circadian and dark-pulse activation of orexin/hypocretin neurons. Molecular Brain

1(1): 19.

McGranaghan, P. A. and H. D. Piggins (2001). Orexin A-like immunoreactivity in the

hypothalamus and thalamus of the Syrian hamster (*Mesocricetus auratus*) and Siberian

hamster (*Phodopus sungorus*), with special reference to circadian structures. Brain Res

904(2): 234-244.

Mieda, M., H. Okamoto and T. Sakurai (2016). Manipulating the Cellular Circadian Period of

Arginine Vasopressin Neurons Alters the Behavioral Circadian Period. Curr Biol **26**(18):

2535-2542.

Mieda, M., D. Ono, E. Hasegawa, H. Okamoto, K. Honma, S. Honma and T. Sakurai (2015). Cellular clocks in AVP neurons of the SCN are critical for interneuronal coupling regulating circadian behavior rhythm. Neuron **85**(5): 1103-1116.

Mistlberger, R. E. (2005). Circadian regulation of sleep in mammals: role of the suprachiasmatic nucleus. Brain Res Brain Res Rev **49**(3): 429-454.

Moore, R. Y. and V. B. Eichler (1972). Loss of a circadian adrenal corticosterone rhythm following suprachiasmatic lesions in the rat. Brain Res **42**(1): 201-206.

Moore, R. Y. and J. C. Speh (1993). GABA is the principal neurotransmitter of the circadian system. Neuroscience Letters **150**(1): 112-116.

Nagel, G., T. Szellas, W. Huhn, S. Kateriya, N. Adeishvili, P. Berthold, D. Ollig, P. Hegemann and E. Bamberg (2003). Channelrhodopsin-2, a directly light-gated cation-selective membrane channel. Proceedings of the National Academy of Sciences **100**(24): 13940-13945.

Nakamura, W. (2012). Circadian regulation of sleep-wake cycles and food anticipation. Brain Nerve **64**(6): 647-656.

Ono, D., Y. Mukai, C. J. Hung, S. Chowdhury, T. Sugiyama and A. Yamanaka (2020). The mammalian circadian pacemaker regulates wakefulness via CRF neurons in the paraventricular nucleus of the hypothalamus. Science Advances **6**(45): eabd0384.

Partch, C. L., C. B. Green and J. S. Takahashi (2014). Molecular architecture of the mammalian circadian clock. Trends Cell Biol **24**(2): 90-99.

Peyron, C., J. Faraco, W. Rogers, B. Ripley, S. Overeem, Y. Charnay, S. Nevsimalova, M.

Aldrich, D. Reynolds, R. Albin, R. Li, M. Hungs, M. Pedrazzoli, M. Padigaru, M.

Kucherlapati, J. Fan, R. Maki, G. J. Lammers, C. Bouras, R. Kucherlapati, S. Nishino and E.

Mignot (2000). A mutation in a case of early onset narcolepsy and a generalized absence of hypocretin peptides in human narcoleptic brains. Nature Medicine **6**(9): 991-997.

Peyron, C., D. K. Tighe, A. N. van den Pol, L. de Lecea, H. C. Heller, J. G. Sutcliffe and T. S. Kilduff (1998). Neurons containing hypocretin (orexin) project to multiple neuronal systems. J Neurosci **18**(23): 9996-10015.

Porkka-Heiskanen, T. and H.-K. Wigren (2020). Molecular mechanisms of (recovery) sleep: lessons from *Drosophila melanogaster*. Current Opinion in Physiology **15**: 192-196.

Reinhard, N., F. K. Schubert, E. Bertolini, N. Hagedorn, G. Manoli, M. Sekiguchi, T. Yoshii, D. Rieger and C. Helfrich-Förster (2022). The Neuronal Circuit of the Dorsal Circadian Clock Neurons in *Drosophila melanogaster*. Front Physiol **13**: 886432.

Sakurai, T. (2007). The neural circuit of orexin (hypocretin): maintaining sleep and wakefulness. Nature Reviews Neuroscience **8**(3): 171-181.

Schubert, F. K., N. Hagedorn, T. Yoshii, C. Helfrich-Forster and D. Rieger (2018). Neuroanatomical details of the lateral neurons of *Drosophila melanogaster* support their functional role in the circadian system. J Comp Neurol **526**(7): 1209-1231.

Schwartz, W. J. and H. Gainer (1977). Suprachiasmatic nucleus: use of ¹⁴C-labeled deoxyglucose uptake as a functional marker. Science **197**(4308): 1089-1091.

Stephan, F. K. and I. Zucker (1972). Circadian rhythms in drinking behavior and locomotor activity of rats are eliminated by hypothalamic lesions. Proc Natl Acad Sci U S A **69**(6): 1583-1586.

Sullivan, D., K. Mizuseki, A. Sorgi and G. Buzsáki (2014). Comparison of Sleep Spindles and Theta Oscillations in the Hippocampus. The Journal of Neuroscience **34**(2): 662-674.

Tackenberg, M. C., J. J. Hughey and D. G. McMahon (2021). Optogenetic stimulation of VIPergic SCN neurons induces photoperiodic-like changes in the mammalian circadian clock. European Journal of Neuroscience **54**(9): 7063-7071.

Takahashi, J. S. (2017). Transcriptional architecture of the mammalian circadian clock. Nat Rev Genet **18**(3): 164-179.

Thannickal, T. C., R. Y. Moore, R. Nienhuis, L. Ramanathan, S. Gulyani, M. Aldrich, M. Cornford and J. M. Siegel (2000). Reduced number of hypocretin neurons in human narcolepsy. Neuron **27**(3): 469-474.

Tomioka, K. and T. Yoshii (2006). Entrainment of *Drosophila* circadian rhythms by temperature cycles. Sleep and Biological Rhythms **4**(3): 240-247.

Tsunematsu, T., T. S. Kilduff, E. S. Boyden, S. Takahashi, M. Tominaga and A. Yamanaka (2011). Acute Optogenetic Silencing of Orexin/Hypocretin Neurons Induces Slow-Wave Sleep in Mice. The Journal of Neuroscience **31**(29): 10529-10539.

Tsunematsu, T., T. Ueno, S. Tabuchi, A. Inutsuka, K. F. Tanaka, H. Hasuwa, T. S. Kilduff, A. Terao and A. Yamanaka (2014). Optogenetic manipulation of activity and temporally controlled cell-specific ablation reveal a role for MCH neurons in sleep/wake regulation. Journal of Neuroscience **34**(20): 6896-6909.

Vadnie, C. A. and C. A. McClung (2017). Circadian Rhythm Disturbances in Mood Disorders: Insights into the Role of the Suprachiasmatic Nucleus. Neural Plast **2017**: 1504507.

Vadnie, C. A., K. A. Petersen, L. A. Eberhardt, M. A. Hildebrand, A. J. Cerwensky, H. Zhang, J. N. Burns, D. D. Becker-Krail, L. M. DePoy, R. W. Logan and C. A. McClung (2021). The

Suprachiasmatic Nucleus Regulates Anxiety-Like Behavior in Mice. Front Neurosci **15**: 765850.

Vyazovskiy, V. V., U. Olcese, Y. M. Lazimy, U. Faraguna, S. K. Esser, J. C. Williams, C. Cirelli and G. Tononi (2009). Cortical Firing and Sleep Homeostasis. Neuron **63**(6): 865-878.

Weaver, D. R. (1998). The Suprachiasmatic Nucleus: A 25-Year Retrospective. Journal of Biological Rhythms **13**(2): 100-112.

Webb, A. B., N. Angelo, J. E. Huettner and E. D. Herzog (2009). Intrinsic, nondeterministic circadian rhythm generation in identified mammalian neurons. Proc Natl Acad Sci U S A **106**(38): 16493-16498.

Weber, F. (2017). Modeling the mammalian sleep cycle. Current Opinion in Neurobiology **46**: 68-75.

Wen, S. a., D. Ma, M. Zhao, L. Xie, Q. Wu, L. Gou, C. Zhu, Y. Fan, H. Wang and J. Yan (2020). Spatiotemporal single-cell analysis of gene expression in the mouse suprachiasmatic nucleus. Nature Neuroscience **23**(3): 456-467.

Whitt, J. P., J. R. Montgomery and A. L. Meredith (2016). BK channel inactivation gates daytime excitability in the circadian clock. Nat Commun **7**: 10837.

Williams, J. C., J. Xu, Z. Lu, A. Klimas, X. Chen, C. M. Ambrosi, I. S. Cohen and E. Entcheva (2013). Computational optogenetics: empirically-derived voltage- and light-sensitive channelrhodopsin-2 model. PLoS Comput Biol **9**(9): e1003220.

Wollnik, F. (1989). Physiology and regulation of biological rhythms in laboratory animals: an overview. Lab Anim **23**(2): 107-125.

- Xu, H., C. L. Gustafson, P. J. Sammons, S. K. Khan, N. C. Parsley, C. Ramanathan, H. W. Lee, A. C. Liu and C. L. Partch (2015). Cryptochrome 1 regulates the circadian clock through dynamic interactions with the BMAL1 C terminus. Nat Struct Mol Biol **22**(6): 476-484.
- Xu, Y., Q. S. Padiath, R. E. Shapiro, C. R. Jones, S. C. Wu, N. Saigoh, K. Saigoh, L. J. Ptáček and Y. H. Fu (2005). Functional consequences of a CK1delta mutation causing familial advanced sleep phase syndrome. Nature **434**(7033): 640-644.
- Yamashita, T. and A. Yamanaka (2017). Lateral hypothalamic circuits for sleep–wake control. Current Opinion in Neurobiology **44**: 94-100.
- Yizhar, O., L. E. Fenno, M. Prigge, F. Schneider, T. J. Davidson, D. J. O'Shea, V. S. Sohal, I. Goshen, J. Finkelstein, J. T. Paz, K. Stehfest, R. Fudim, C. Ramakrishnan, J. R. Huguenard, P. Hegemann and K. Deisseroth (2011). Neocortical excitation/inhibition balance in information processing and social dysfunction. Nature **477**(7363): 171-178.
- Yoshii, T., D. Rieger and C. Helfrich-Förster (2012). Two clocks in the brain: an update of the morning and evening oscillator model in *Drosophila*. Progress in brain research **199**: 59-82.
- Zant, J. C., T. Kim, L. Prokai, S. Szarka, J. McNally, J. T. McKenna, C. Shukla, C. Yang, A. V. Kalinchuk, R. W. McCarley, R. E. Brown and R. Basheer (2016). Cholinergic Neurons in the Basal Forebrain Promote Wakefulness by Actions on Neighboring Non-Cholinergic Neurons: An Opto-Dialysis Study. The Journal of Neuroscience **36**(6): 2057-2067.
- Zhang, F., V. Gradinaru, A. R. Adamantidis, R. Durand, R. D. Airan, L. de Lecea and K. Deisseroth (2010). Optogenetic interrogation of neural circuits: technology for probing mammalian brain structures. Nat Protoc **5**(3): 439-456.

Key resource table

REAGENT or RESOURCE	SOURCE	IDENTIFIER
Antibodies		
Rabbit anti-GFP	Thermo Fisher Scientific	Cat#A11122
Donkey anti-rabbit IgG, Alexa Fluor 488	Thermo Fisher Scientific	Cat#A21206
Virus Strains		
AAV-EF1a-DIO-SSFO-EYFP	Addgene	Cat#35503
AAV-hSyn-hChR2(H134R)-EYFP	This study	NA
AAV-EF1a-DIO-mCherry	Addgene	Cat#50462
Experimental Models: Organisms/Strains		
AVP-Cre mice	Kanazawa University, Department of Integrative Neurophysiology	NA
VIP-Cre mice	Jackson Laboratory, Bar Harbor, ME USA	JAX #010908
Software and Algorithms		
R Studio Desktop	RStudio	https://www.rstudio.com/
SleepSign Version 3.0	Kissei Comtec Co., Ltd.	http://www.sleepsign.com/
VitalRecorder	Kissei Comtec Co., Ltd.	http://www.sleepsign.com/
Adobe Illustrator 2022	Adobe	https://www.adobe.com/
Adobe Photoshop 2022	Adobe	https://www.adobe.com/

Attachments

Attachment 1 : Protocol AAV generation

1 of 8

Project created on 12.03.2018 15:49.

Report for project A new look at the role of AVP neurons in the pacemaking of the SCN

Experiment created on 07.05.2018 03:54.

AAV Generation

Construction of functional pAAV virus in order to express the desired optogenetic construct in targeted cells.

Task created on 07.05.2018 06:06.

Cell culture

Due date: 07.05.2018 14:00 Completed on 07.05.2018 06:24

Culturing host cells to facilitated the initial production, amplification and titering of replication-incompetent adenovirus.

Task tags: Department of Integrative Neurophysiology, Kanazawa University

Completed by Florian Rumpf on 09.05.2018 01:11.

Step 1: Medium preparation Completed

Work on sterile bench!

1. 500ml D-MEM (High glucose, eg. Sigma D5796)
2. 50ml fetal bovine serum
3. 5ml 2mM L-glutamine
4. 2,5ml Penicillin-streptomycin 25 U/ml

Comments for step Medium preparation

No comments

Completed by Florian Rumpf on 09.05.2018 01:11.

Step 2: Cell spreading Completed

Work on sterile bench!

1. Fibroblast Cell line (293A) from cold storage
2. Add 5ml of Medium
3. Centrifuge at 700 RPM 8min
4. Suck medium out while leaving cell pellet in the testtube with a sterile pump
5. Resuspend cells in 5ml of medium
6. Put in petri dish (Coated surface petri dish - Nunclon Delta surface) with 5ml more of medium (volume for a 10cm dish => total filling of 10ml)
7. Carefully mix while maintaining even spread of cells
8. Incubate at 37°C / 5% CO2

Comments for step Cell spreading

No comments

Completed by Florian Rumpf on 09.05.2018 07:09.

Step 3: Cell splitting Completed

Work on sterile bench!

- Split the cells to new dish when 75% confluence is reached (ca. 48h).
 - 4.5×10^5 seeded → confluent after 4 days
 - 6.5×10^5 seeded → confluent after 3 days
 - 1×10^6 seeded → confluent after 2 days
1. Unfreeze Trypsin-EDTA
 2. Turn on hood, gas and microscope
 3. Sterilize pipet (alcohol + burn)
 4. Aspirate medium
 5. Wash in 4ml PBS
 6. Aspirate PBS
 7. Apply 0.5ml Trypsin-EDTA to detach cells from dish (ca 2 min - check under microscope)
 8. Add 10ml of medium
 9. Mix by pipeting (don't fully empty the dish/pipet to avoid bubbles -> cell lysing)
 10. Prepare cell counter
 11. Add small amount of solution (50 μ L) to counter
 12. Count cells under microscope $\text{cells}/0.1 \text{ mm}^3 = \text{cells}/10^{-4} \text{ ml}$ (e.g. $15/0.1 \text{ mm}^3 = 1.5 \times 10^6/10 \text{ ml}$)
 13. Seed dishes according to the amount of cells you have counted (e.g. $4 \times 10^6/10 \text{ ml}$ counted → makes 4 dishes seeded with $1 \times 10^6/10 \text{ ml}$ each)
 14. Clean counter, pipet and workspace
 15. Turn off light, gas, hood and microscope

Comments for step Cell splitting

No comments

Task created on 07.05.2018 04:08.

Plasmid Preparation

No due date Completed on 09.05.2018 03:50

Thanks to Prof. Nagel from the University of Wuerzburg for providing the purified pAAV cis vector.

Task tags: Department of Integrative Neurophysiology, Kanazawa University

Completed by Florian Rumpf on 09.05.2018 03:49.

Step 1: Construction Completed

pAAV cis vector: Promoter + FLEX + Gene to be expressed + cDNA + WPRE + polyA

Because ITR is included in the vector that incorporates the expression unit, recombination tends to occur between ITRs in ordinary Escherichia coli strains (DH5a etc.). All of the plasmids containing ITR are prepared using either Sibl 2, Sibl 3 strain (Invitrogen), or NEB stable strain to that no deletion occurs in the process.

[Production and Titring of Recombinant Adeno-as...] File uploaded on 07.05.2018 06:01.

[AAV160909.doc] File uploaded on 07.05.2018 06:01.

[Übersetzung AAV Protocol.docx] File uploaded on 07.05.2018 06:01.

Comments for step Construction

No comments

Completed by Florian Rumpf on 09.05.2018 03:49.

Step 2: Plasmid purification Completed

10 µg of each plasmid is needed at a concentration of 1 µg/µl

Comments for step Plasmid purification

No comments

Task created on 07.05.2018 04:08.

Packaging

Due date: 15.05.2018 14:00 Completed on 17.05.2018 01:55

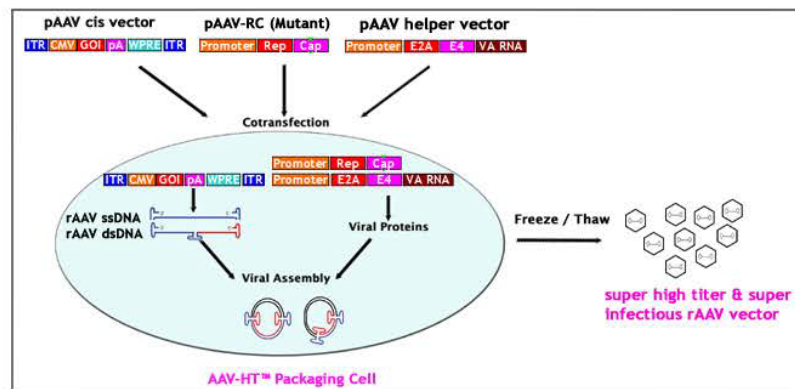
3 kinds of plasmids are cotransfected into 293 A cells (Invitrogen) by calcium phosphate method.

Task tags: Department of Integrative Neurophysiology, Kanazawa University

Completed by Florian Rumpf on 15.05.2018 04:58.

Step 1: Overview Completed

- 3 kinds of plasmids are needed.
 - pAAV cis vector (expression unit): Promoter + FLEX + Gene to be expressed + cDNA +WPRE + polyA
 - pAAV-RC (Capsid serotype 2 - serotype 10 according to targeted cells)
 - pAAV helper vector
- Cotransfection of the plasmids into 293 A cells (Invitrogen) by calcium phosphate method
 - With this method it is possible to obtain a virus titer which is considerably higher than that of lipofection (Fugene et al.). Lipofection is considered to be one of the reasons that the amount of plasmid is small.



Comments for step Overview

No comments

Completed by Florian Rumpf on 15.05.2018 05:44.

➔ **Step 2: Plasmid selection** Completed

pAAV-doubleflexed-ChR2-EYFP (GFP derived) concentrated to 1 µg/µl

pAAV-rh10 (M0223) concentrated to 1 µg/µl

pHelper concentrated to 1 µg/µl

Comments for step Plasmid selection

No comments

Completed by Florian Rumpf on 15.05.2018 04:58.

➔ **Step 3: Cell spreading** Completed

24h before transfection 293A cells are spread on four 10cm dishes at 4.5×10^6 cells / dish in 10ml medium / dish. Thereby >90% confluence is achieved on the next day.

Important:

- Even spread of cells
- At time of transfection it is preferable that the plate is almost filled with cells, but contact inhibition is not yet apparent.

Comments for step Cell spreading

No comments

Completed by Florian Rumpf on 15.05.2018 05:01.

➔ **Step 4: Solution preparation** Completed

1. 0.3 M CaCl₂

- a. CaCl₂ · 2 H₂O 22.052g /500 ml (CaCl₂ must be melted separately before it dissolves)
- b. filter sterilization at 4 °C

2. 2 × HBS

- a. 8.182g NaCl
- b. 0.106 g Na₂HPO₄
- c. 5.958g / 500 ml HEPES
- d. pH 7.10 (Since the pH is slightly increased by filter sterilization, try to achieve a pH of 7.06 and compare the efficiency of the transfection)
- e. filter sterilization at 4 °C

Comments for step Solution preparation

No comments

Completed by Florian Rumpf on 15.05.2018 05:44.

➔ **Step 5: Plasmid preparation** Completed

- Prepare 50ml tube with 4ml 0.3 M CaCl₂
- Prepare 50ml tube with 4ml of 2xHBS
- Add all three plasmids (40 µg each) to the tube containing CaCl₂
- Plasmid/ CaCl₂ solution is added dropwise to 2xHBS with slow stirring. Then stir by pipetting.
- Leave at room temperature for 20 minutes

Comments for step Plasmid preparation

Florian Rumpf on 15.05.2018 at 05:03:

Precipitation of Calciumphosphate with DNA enclosed → cell take up

Completed by Florian Rumpf on 15.05.2018 05:58.

➔ **Step 6: Introduction of plasmids to dishes** Completed

- Apply 2ml of Plasmid / CaCl₂ / HBS solution slowly and evenly to the four dishes.
- Incubate at 37°C overnight

Comments for step Introduction of plasmids to dishes

No comments

Completed by Florian Rumpf on 17.05.2018 01:55.

➔ **Step 7: Change medium** Completed

- Change the medium the next day
- Incubate overnight

Comments for step Change medium

No comments

Completed by Florian Rumpf on 18.05.2018 02:12.

➔ **Step 8: Cell collection** Completed

3 days after the start of transfection the cells are collected. All waste from these steps must be collected for autoclave!

- Peel off the cells with a scraper and collect the cells suspended in medium from all dishes in one tube (4 dishes → 50ml tube)
- Percipitate the cells by low speed centrifugation (24°C, 800 RPM, 8min)
- Remove medium and collect as special waste
- Resuspend pellet in 10ml of PBS
- Percipitate again by low speed centrifugation (24°C, 800 RPM, 8min)
- Remove supernatant collect as special waste
- Resuspend in 100µL per dish of PBS-MK (PBS + Sigma D 8537 1 mM MgCl₂)
- Transfer to cryotube and freeze with liquid nitrogen (It can also be stored at -80 °C)

Comments for step Cell collection

No comments

Task created on 07.05.2018 04:08.

 **Extraction**

No due date Completed on 18.05.2018 06:05

High concentration of replication-incompetent AAV is extracted from the host cells.

Task tags: Department of Integrative Neurophysiology, Kanazawa University

Completed by Florian Rumpf on 18.05.2018 04:58.

➔ **Step 1: Cell Lysing** Completed

- Frozen infected cells are thawed at 37°C
- Freeze thaw is repeated once again (twice in total)
- After thawing, stir with vortex for 1 minute
- Centrifuge at 15,000 rpm, 5 min, 4°C
- Collect the supernatant in a 1.5 mL tube

Comments for step Cell Lysing

No comments

Completed by Florian Rumpf on 18.05.2018 06:05.

Step 2: Low scale purification Completed

- Add 1 μ l of Benzonase to the collected supernatant (Benzonase Nuclease HC: Novagen, Purity > 90%, #71205, 25 kU, 250 U / μ L)
- Incubate at 37°C for 30 min
- Centrifuge at 15,000 rpm, 5 min, 4°C
- Collect the supernatant in a 1.5mL tube
- Repeat: Centrifuge at 15,000 rpm, 5 min, 4°C once more
- Collect the supernatant in a 1.5mL tube

Comments for step Low scale purification

No comments

Completed by Florian Rumpf on 18.05.2018 06:05.

Step 3: Storage Completed

- Apportion the collected material (5 μ L or 50 μ L)
- Quickly freeze with liquid nitrogen and store at -80°C

Comments for step Storage

No comments

Task created on 09.05.2018 01:09.

Titer measurement

Due date: 18.05.2018 17:00 Completed on 25.05.2018 07:25


Titer measurement via quantitative PCR.

Task tags: Department of Integrative Neurophysiology, Kanazawa University

Completed by Florian Rumpf on 18.05.2018 07:03.

Step 1: Virus dilution Completed

1. Main power supply of Light Cycler is kept ON (back side of main unit side)
2. Prepare a 1,5ml tube with 100 μ l of 50 mM NaOH
3. 2 μ l of the remaining virus is added
4. Incubate at 95 ° C for 30 min
5. Add 8.4 μ l of 1 M Tris-HCl (Ph 8.0) → ★
6. Take 2 μ l from ★, add 38 μ l of 10 mM TH 8.0 without EDTA (= Dilution of 1:20) → □

 [Titer_measurement → Quantitative_PCR_(1).docx] File uploaded on 17.05.2018 03:01.

Comments for step Virus dilution

No comments

Completed by Florian Rumpf on 25.05.2018 03:57.

Step 2: Master mix preparation CompletedMaster Mix is prepared at 7.5 μ l for each well that needs to be filled

→ [Standard solutions (1/1, 1/10, 1/100, 1/1000) + number of samples] × 2 + 1

(Fluorescent Probe solution hybridizes with specific primer sequence in the virus DNA during PCR cycling. This makes the PCR live quantifiable)

[Master mix for one well sample] Table created on 17.05.2018 02:41.

	A	B	C
1		Vol.	Storage location
2	Distilled H ₂ O	1.5µl	In the shelf of the freezer G, inside the front box
3	10mM AAV-WPRE-LC1	0.5µl	In the freezer C, paper box
4	10mM AAV-WPRE-LC2	0.5µl	In the freezer C, paper box
5	Probe #77	0.1µl	Metallic tube of the back of freezer G
6	2x Master Put in last and then mix the solution	5.0µl	In the shelf of freezer G, inside the front box

Comments for step Master mix preparation

No comments

Completed by Florian Rumpf on 25.05.2018 03:57.

➤ Step 3: Virus standard Completed

Standard virus for later reference is prepared at 4 dilution stages. Starting with a concentration of 10^8 / 2.5µl and create 1/10, 1/100 and 1/1000 dilutions.

Comments for step Virus standard

No comments

Completed by Florian Rumpf on 25.05.2018 03:57.

➤ Step 4: Well filling Completed

- 7.5 µl Master Mix + 2.5 µl diluted DNA (□) = 10 µl

- Put the master mix in well
- Seal the top of the well with plastic film
- Place DNA in the top of the well and centrifuge (room temperature, 500 rpm, 30 seconds)



Comments for step Well filling

No comments

Completed by Florian Rumpf on 25.05.2018 03:57.

➤ Step 5: PCR system initiation Completed

- Press the ← → button on the Light Cycler, put the well into the main unit, press ← → button, (green light)
- Start the PC with a blank password after starting the main unit
- start the Light Cycler program
User: admin

Pass: Master 1

✓

4. New Experiment from Template
 - a. AAV-CAG Run Protocol → ✓
 - b. Amplification changed to 55 cycle (default is 45 each time)
 - c. Start cycling
5. As you are asked where to save the data, go to the Root / System / Admin / Experiments folder
→ Name the file including the date and name of virus sample ✓
6. Subset Editor
 - a. Press (+) under Subsets
 - b. Mark the wells containing samples on the right side
7. Sample Editor
 - a. Select workflow Abs Quant for absolute quantification
 - b. Select the samples from your created subset
 - c. Use the well editor to modify the seeded wells
 - α. Enter quantification sample type „Standard“ for the standards
 - β. Enter a sample name for each well
 - γ. Enter the seeded concentrations for the standards

Comments for step PCR system initiation

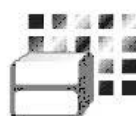
No comments

Completed by Florian Rumpf on 25.05.2018 07:25.

➔ **Step 6: Results** Completed

1. Analysis
 - a. Abs Quant / 2nd Derivative Max
 - b. Subset → New subset 1 → ✓ (To 3 if no results are obtained)
 - c. calculate
 - d.
 - e. When the result comes out, right-click on the sample table → export table as textfile
 - a. Press floppy symbol
 - b. Report subset
 - c. Generate
 - d. Press PDF and save
1. When no result is obtained
 - a. Press + on Analysis on ±
 - b. Set Analysis type to Abs Quant / Fit point. Select Subset ✓
 - c. Set the Noise Band in a place parallel to Calculate

Attachment 2 : Quantitative PCR results



LightCycler® 480 Software

Report



180528EYFP-CHR2&EYFP

Experiment

Creation Date	5/28/2018 11:23:30 AM	Last Modified Date	5/28/2018 2:25:58 PM
Operator	System Admin	Owner	System Admin
Start Time	5/28/2018 11:26:37 AM	End Time	5/28/2018 12:55:01 PM
Run State	Completed	Software Version	LC S480 1.5.0.39
Macro		Macro Owner	
Macro Status			
Templates	AAV-CAG Run Protocol	Plate ID	02557307
Test ID		Lot ID	
Color Comp ID			
Run Notes			

Programs

Program Name	pre-incubation						
Cycles	1	Analysis Mode	None				
Target (°C)	Acquisition Mode	Hold (hh:mm:ss)	Ramp Rate (°C/s)	Acquisitions (per °C)	Sec Target (°C)	Step size (°C)	Step Delay (cycles)
95	None	00:10:00	4.40		0	0	0
Program Name	amplification						
Cycles	55	Analysis Mode	Quantification				
Target (°C)	Acquisition Mode	Hold (hh:mm:ss)	Ramp Rate (°C/s)	Acquisitions (per °C)	Sec Target (°C)	Step size (°C)	Step Delay (cycles)
95	None	00:00:10	4.40		0	0	0
55	None	00:00:30	2.20		0	0	0
72	Single	00:00:01	4.40		0	0	0
Program Name	cooling						
Cycles	1	Analysis Mode	None				
Target (°C)	Acquisition Mode	Hold (hh:mm:ss)	Ramp Rate (°C/s)	Acquisitions (per °C)	Sec Target (°C)	Step size (°C)	Step Delay (cycles)
40	None	00:00:30	2.20		0	0	0

Samples

Sample Count	12			
Subset	New Subset 1			
Pos	Name	ID	Repl. Of	Sample Notes
A3	Sample 3			
A4	Sample 4			

Samples

Sample Count	12			
Subset	New Subset 1			
Pos	Name	ID	Repl. Of	Sample Notes
B3	Sample 15			
B4	Sample 16			
C3	Sample 27			
C4	Sample 28			
D3	Sample 39			
D4	Sample 40			
E3	mCherry			
E4	mCherry			
F3	ChR2-EYFP			
F4	ChR2-EYFP			

Revision History

Revision	Date	User	Reason

Abs Quant/2nd Derivative Max for New Subset 1 (Abs Quant/2nd Derivative Max)**Settings**

Channel	465-510		
Color Compensation	Off		
Program	amplification	Units	
Mode	High Confidence		

Subset Name	New Subset 1
-------------	--------------

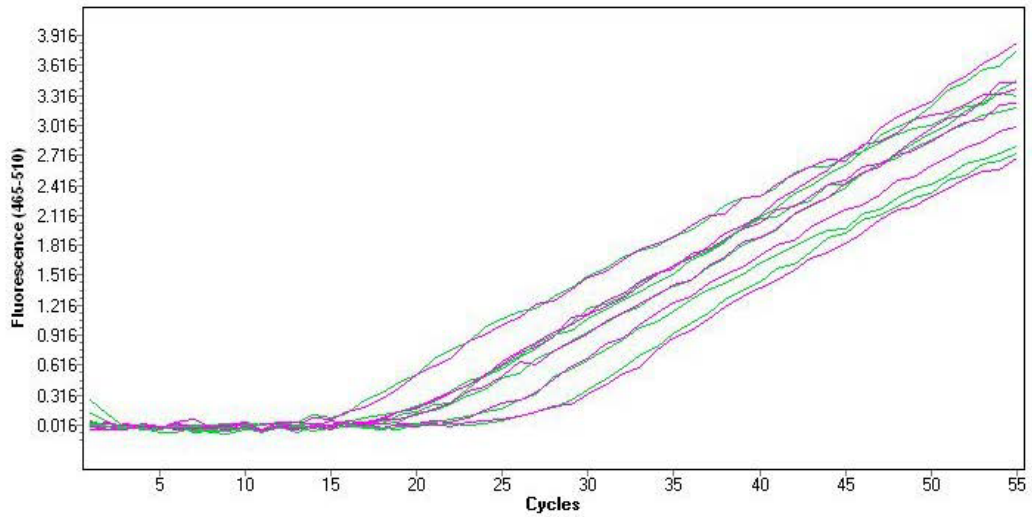
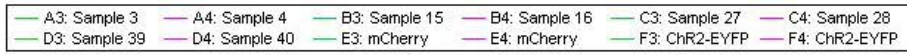
Results

Inc	Pos	Name	Type	CP	Concentration	Standard	Status
<input checked="" type="checkbox"/>	A3	Sample 3	Standard	15.93	7.82E7	1.00E8	
<input checked="" type="checkbox"/>	A4	Sample 4	Standard	16.46	6.00E7	1.00E8	
<input checked="" type="checkbox"/>	B3	Sample 15	Standard	20.37	8.45E6	1.00E7	
<input checked="" type="checkbox"/>	B4	Sample 16	Standard	17.50	3.55E7	1.00E7	
<input checked="" type="checkbox"/>	C3	Sample 27	Standard	25.28	7.23E5	1.00E6	
<input checked="" type="checkbox"/>	C4	Sample 28	Standard	24.67	9.80E5	1.00E6	
<input checked="" type="checkbox"/>	D3	Sample 39	Standard	27.53	2.34E5	1.00E5	
<input checked="" type="checkbox"/>	D4	Sample 40	Standard	29.03	1.10E5	1.00E5	
<input checked="" type="checkbox"/>	E3	mCherry	Unknown	19.30	1.45E7		
<input checked="" type="checkbox"/>	E4	mCherry	Unknown	18.67	1.98E7		
<input checked="" type="checkbox"/>	F3	ChR2-EYFP	Unknown	20.04	9.95E6		

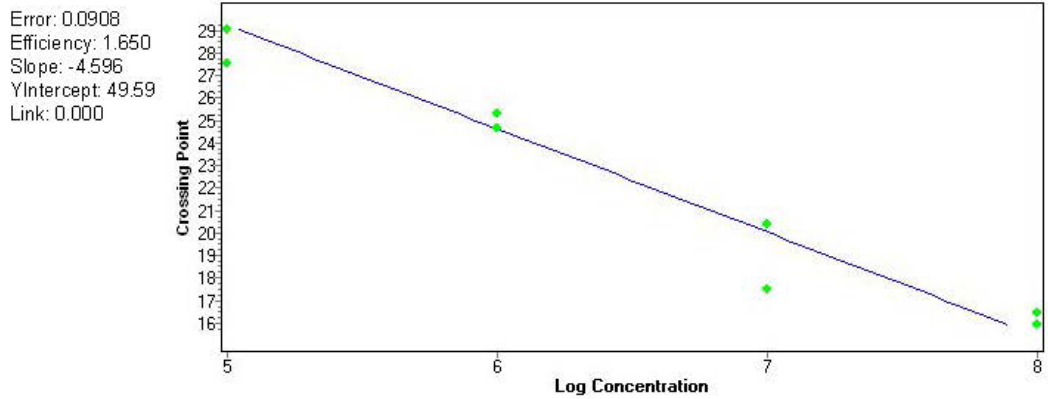
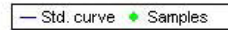
Results

Inc	Pos	Name	Type	CP	Concentration	Standard	Status
<input checked="" type="checkbox"/>	F4	Chr2-EYFP	Unknown				

Amplification Curves



Standard Curve

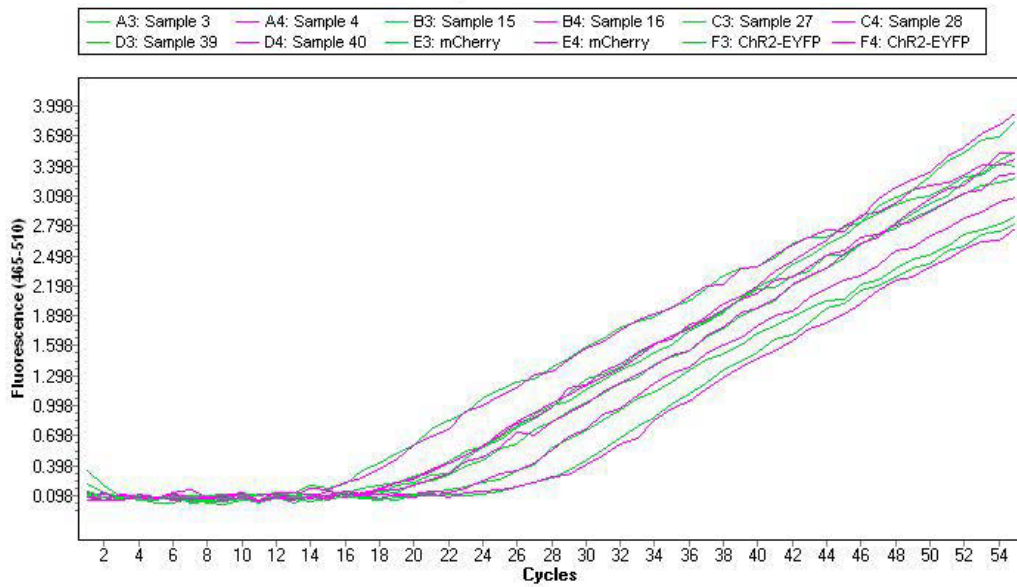


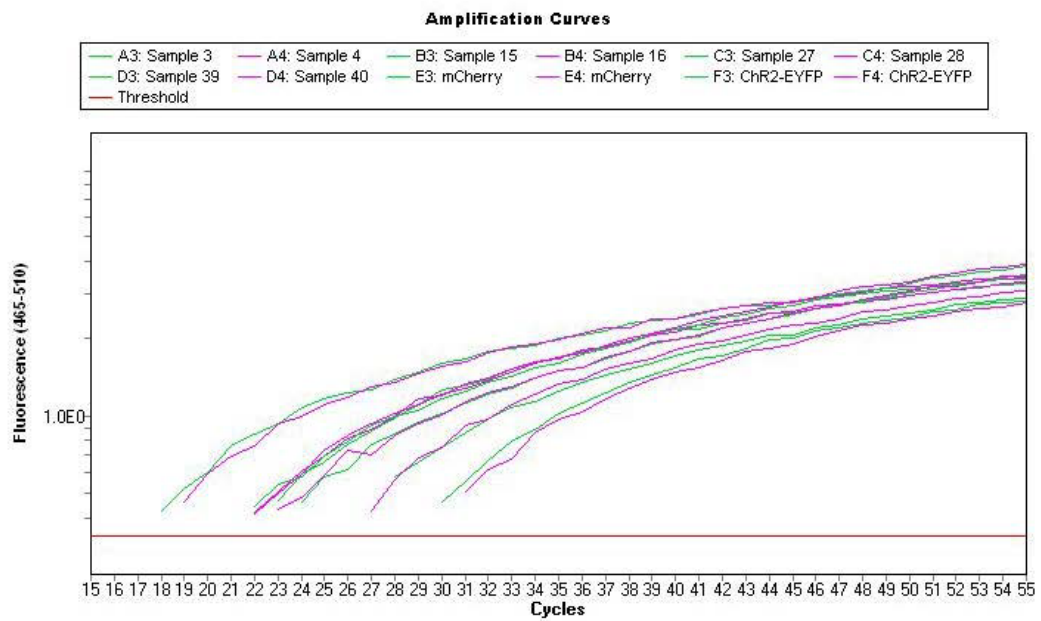
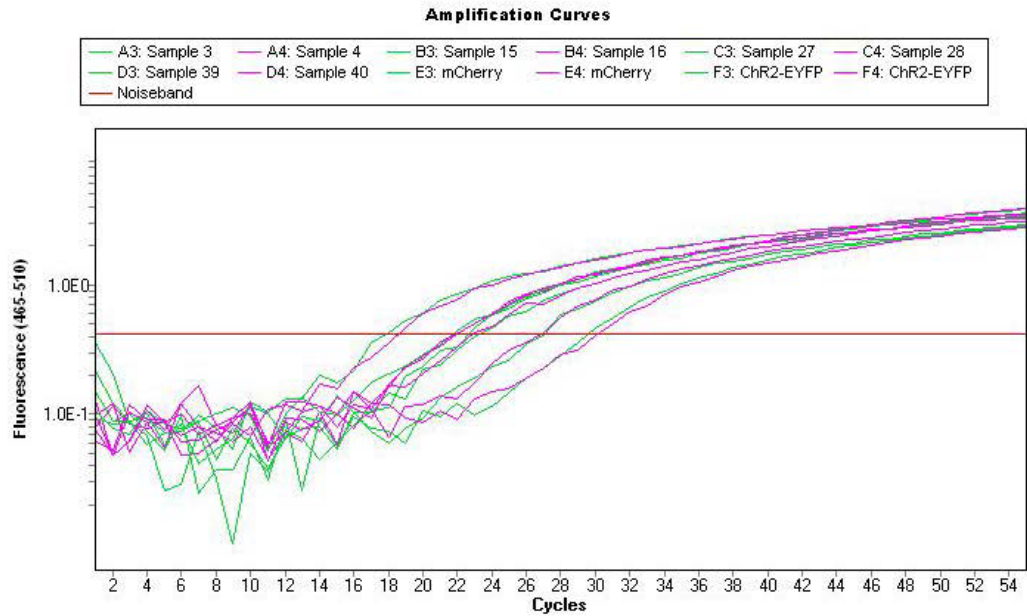
Abs Quant/Fit Points for New Subset 1 (Abs Quant/Fit Points)

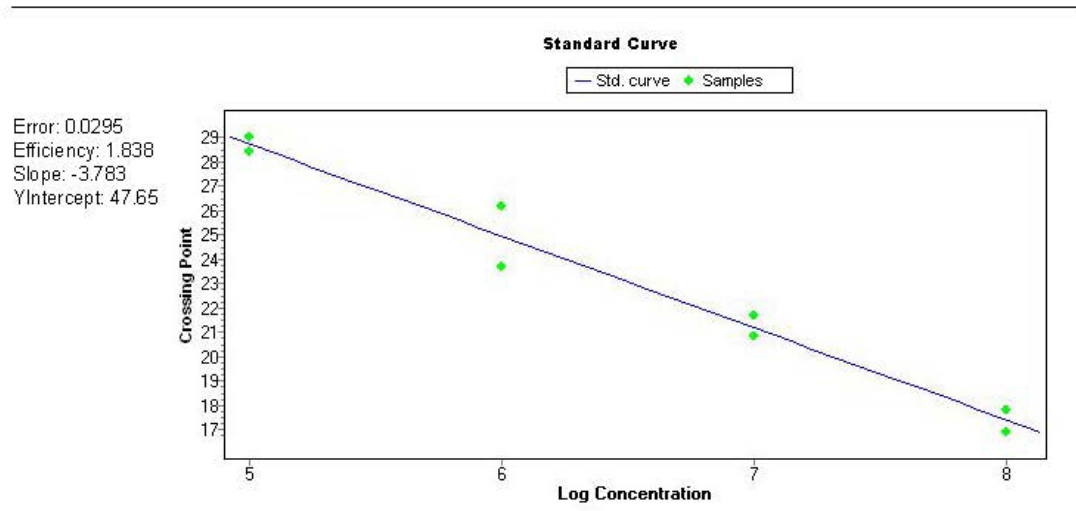
Results

Inc	Pos	Name	Type	CP	Concentration	Standard	Status
<input checked="" type="checkbox"/>	A3	Sample 3	Standard	16.88	1.36E8	1.00E8	
<input checked="" type="checkbox"/>	A4	Sample 4	Standard	17.78	7.86E7	1.00E8	
<input checked="" type="checkbox"/>	B3	Sample 15	Standard	21.69	7.27E6	1.00E7	
<input checked="" type="checkbox"/>	B4	Sample 16	Standard	20.84	1.22E7	1.00E7	
<input checked="" type="checkbox"/>	C3	Sample 27	Standard	23.68	2.17E6	1.00E6	
<input checked="" type="checkbox"/>	C4	Sample 28	Standard	26.18	4.75E5	1.00E6	
<input checked="" type="checkbox"/>	D3	Sample 39	Standard	28.41	1.22E5	1.00E5	
<input checked="" type="checkbox"/>	D4	Sample 40	Standard	29.03	8.38E4	1.00E5	
<input checked="" type="checkbox"/>	E3	mCherry	Unknown	20.62	1.40E7		
<input checked="" type="checkbox"/>	E4	mCherry	Unknown	20.87	1.20E7		
<input checked="" type="checkbox"/>	F3	Chr2-EYFP	Unknown	22.66	4.03E6		
<input checked="" type="checkbox"/>	F4	Chr2-EYFP	Unknown	20.79	1.26E7		

Amplification Curves







Attachment 3 : Protocol for AAV injections and implant surgery**Equipment preparation**

1. Injection-Needle (Glas electrode or Hamilton syringe)
2. Sedan: GABA-Agonist (Benzodiazepem) + α 2-Adren.-Agonist + Synthetic opioid => 2h knockout
3. Antisedan: α 2-Adren.-Antagonist
4. Adenovirus on ice
5. EEG/EMG Implant
6. Optic fiber cannula
7. Disinfectant (Iodid)
8. Other solutions that are out of stock in the operation room

Mouse preparation

1. Check weight of mouse & note
2. Put mouse in separate cage
3. Inject mouse with 0.1 ml sedan per 10g bodyweight intraperitoneally
 1. Prepare injection
 2. Grab mouse by the neck
 3. Inject ventrally from the right side
 4. Aspirate -> air -> IP
4. Wait & Check pain reflex on mouse by gripping the paws with forceps
5. When mouse doesn't show a pain reflex anymore continue
6. Use cutting machine, scissors and hair removing cream to remove the hair from the back of the skull

Sedan = mixture of three anesthetics and analgesics:

- Medetomidine (trade name: Domitor), an α 2 adrenergic agonist
- Midazolam (trade name: Dormicum), a benzodiazepine
- Butorphanol (trade name: Vetorphale), a synthetic opioid

Fixture of mouse to stereotactic frame

1. Stabilize the head by loosely fixing it to the nose clamp
2. Loosely put the ear bars on both sides of the head where you expect the external acoustic porus to be
3. Insert the individual ear bars carefully on each side
4. Check proper positioning by moving the nose clamp -> if the ear bars are properly inserted you can rotate the head up and down but there is no lateral movement
5. Adjust the position of the bars to move the head into the most central position

Craniectomy

1. Disinfect skin with iodid
2. Cut the skin sagittally
3. Disinfect opening with Peroxid

4. Spread opening with cotton swabs and dry skull to see sutures
5. Adjust ear bar height so that Bregma and Lambda are horizontal and the sagittal suture and the nose bar form one line
6. Use a dental drill to drill holes according to stereotactic coordinates
7. Use a needle to pull the bone fragments to the lateral side of the hole
8. Dry hole with paper swabs
9. Insert disinfected screws into holes (~1.5 turns)

Needle preparation

1. Expose 1 cm from the tip of the needle by pulling back the stopper
2. Attach the auto-injector to the stereotaxic frame
3. Wash syringe 2x with 70% EtOH and once with Saline
4. Set the settings of the auto-injector to table = Hamilton 1700 and Wdw: volume = 1 μ l, rate = 1 μ l/min
5. Put the tip of the needle into the virus solution (should be stored in the freezer until now)
6. Press Run

Virus injection

1. Guide the needle to the correct injection site by using the coordinates from a brain atlas. The following coordinates were used:
 1. Bregma = -0.5mm
 2. Lateral = 0.25mm
 3. Depth = 5.5mm
2. Insert the needle and check with the binocular if the dura breaks (Puncture with extra glass electrode if necessary)
3. Slowly apply the virus (Hamilton syringe: 0.1 μ l/min)
4. After completion leave the needle in place for another 10 minutes
5. Pull out the needle

Implant optic fiber

1. Attach the holder for the optical ferrule to the stereotaxic frame
2. Guide the ferrule to the correct position according to brain atlas measurements
3. Use dental glue to fix the cannula in place

Optical implant specifications:

Ferrule diameter: 1.25mm

Length: 6mm +/- 0.5mm

Optic fiber diameter: 200 μ m

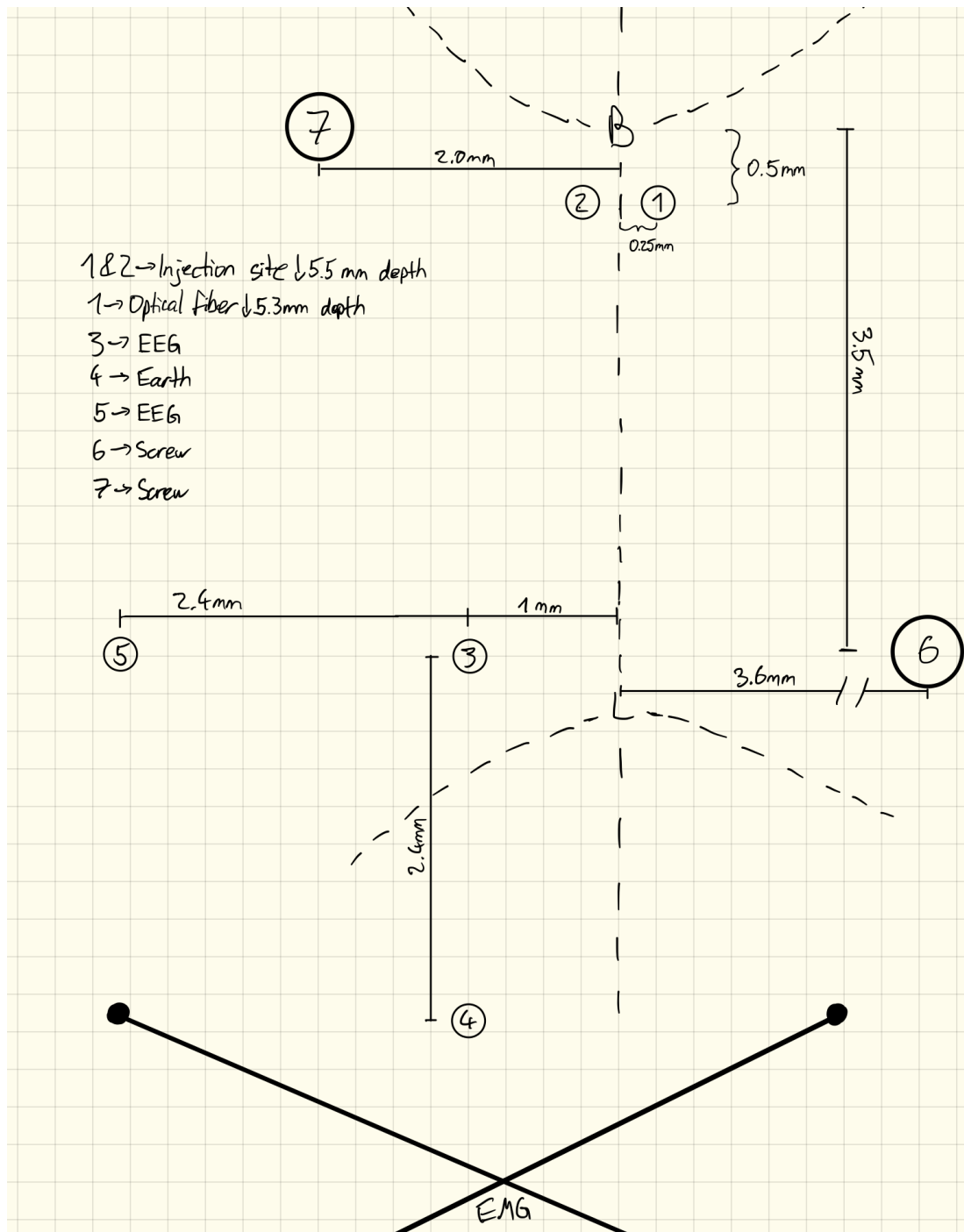
Implant EEG/EMG electrodes

1. Put the EEG-implant electrodes in the predrilled holes
2. Use dental cement to fix the implant to the skull
3. Put the EMG electrodes on the nuchal muscles

Finalize implant

1. Cover all exposed skull surface with dental cement
2. Pull the skin over the dental cement
3. Apply antibiotic cream to the outside of the operation site

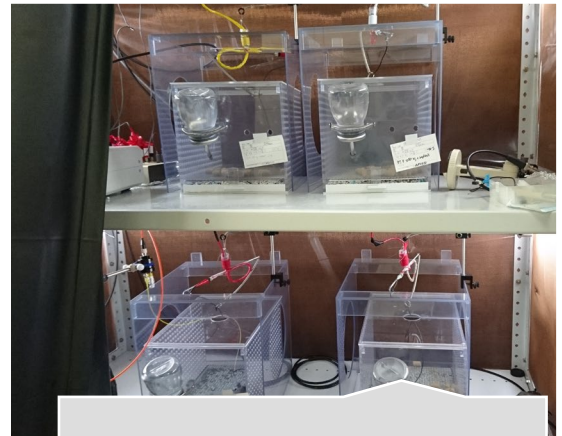
Attachment 4 : Implant map



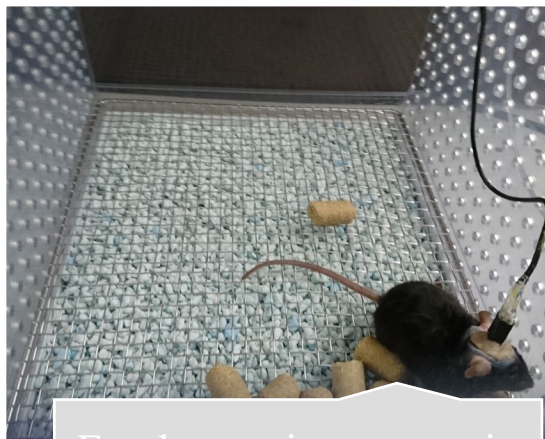
Attachment 5 : Recording setup photos



Raspberry Pi



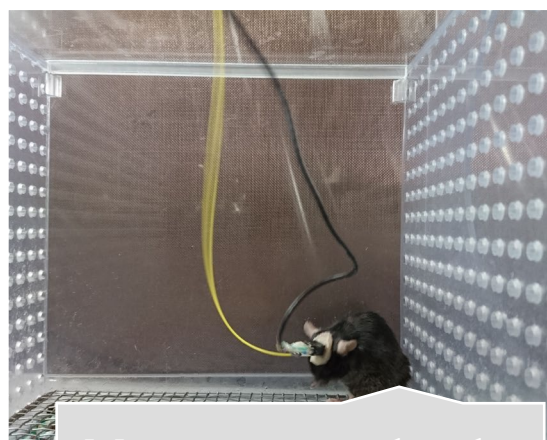
Recording Chambers



Freely moving mouse in recording chamber #1



Freely moving mouse in recording chamber #2



Mouse connected to the laser via optic fiber

Attachment 6 : Python program ChR2

```

import RPi.GPIO as GPIO
import time

GPIO.setwarnings(False) #pin setup
GPIO.setmode(GPIO.BOARD)
GPIO.setup(12,GPIO.OUT)
GPIO.setup(18,GPIO.OUT)

GPIO.output(18, True) #switch on relay connected to pin 18

time.sleep(300) #let laser warm up for 5 minutes

def beep(repeat):
    for i in range(0, repeat):
        for pulse in range(28800): # square wave loop that blinks
            at a frequency of 8 Hz for 1 hour
                GPIO.output(12, True)
                time.sleep(0.0625) # high for .0625 sec
                GPIO.output(12, False)
                time.sleep(0.0625) # low for .0625 sec
beep(1)

GPIO.output(18, False) #switch off relay

GPIO.cleanup()

```

Attachment 7 : Python program SSFO

```

import RPi.GPIO as GPIO
import time

GPIO.setwarnings(False)
GPIO.setmode(GPIO.BOARD)
GPIO.setup(12,GPIO.OUT)
GPIO.setup(18,GPIO.OUT)

GPIO.output(18, True)

time.sleep(300)

def beep(repeat):
    for i in range(0, repeat):
        for pulse in range(3): # square wave loop
            GPIO.output(12, True)
            time.sleep(2) # high for 2 sec
            GPIO.output(12, False)
            time.sleep(1200) # low for 20 min
beep(1)

GPIO.output(18, False)

GPIO.cleanup()

```

Attachment 8 : Sleep sign screening logic

State	Lower 1	Parameter 1	Upper 1	Lower 2	Parameter 2	Upper 2
W	≥ 0.150	EMG Integral	≤ 10000			
R	> 0	EEG Integral	≤ 7000	> 50	FFT-Theta-Ratio	≤ 100
S	> 50	FFT-Delta-Ratio	≤ 100	> 0	FFT-Theta-Ratio	≤ 30
S	*					

* unclassifiable measurements were scored as sleep during screening

S = Non-REM sleep, R = REM sleep, W = wake

Attachment 9 : Cutting solution

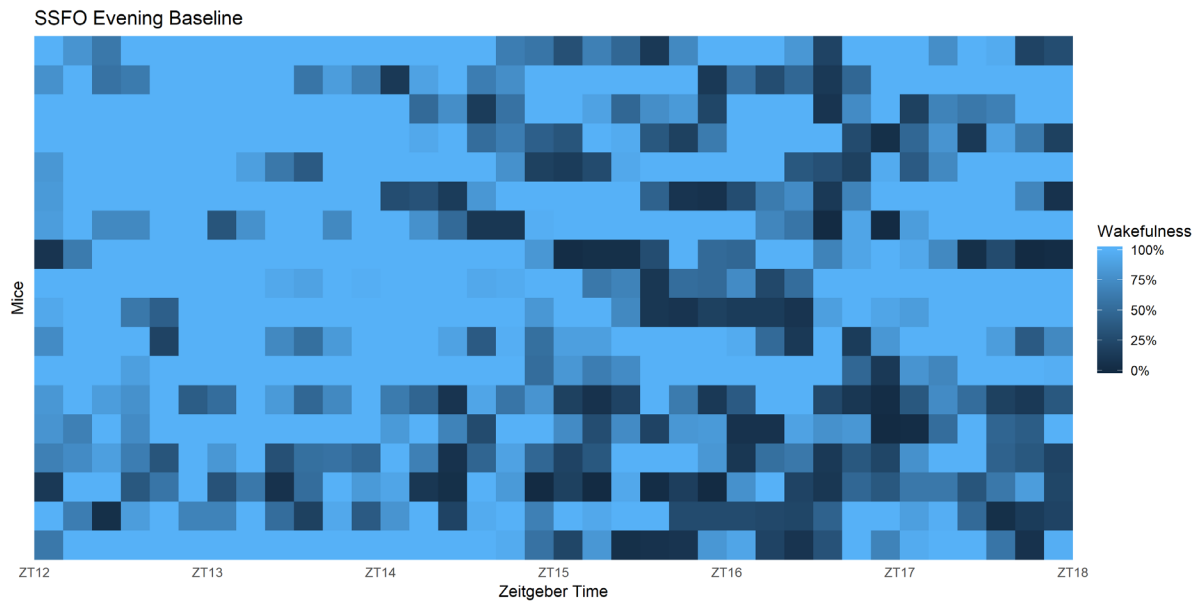
Chemical	mM	Molecular weight
NaCl	87	58.44
Sucrose	75	342.3
KCl	2.5	74.55
NaH₂PO₄(H₂O)₂	1.25	156.01
NaHCO₃	25	84.01
CaCl₂	0.5	110.98
MgCl₂(H₂O)₆	7	203.3
D(+)-Glucose	10	180.16
O₂ 95%	-	-
CO₂ 5%	-	-

Attachment 10 : External recording solution

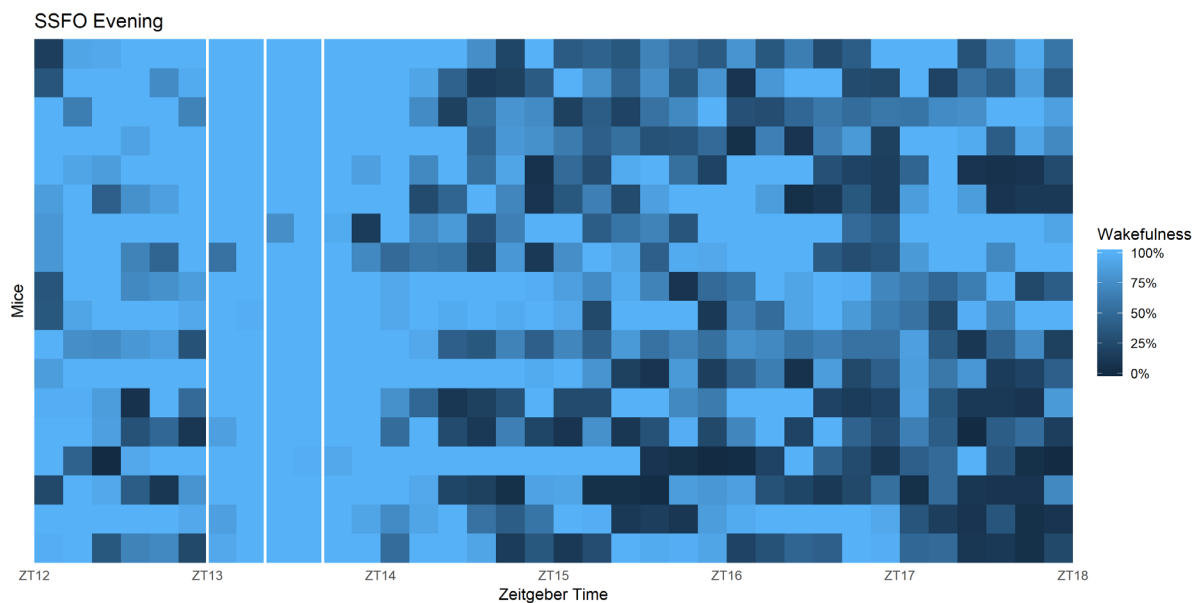
Chemical	mM	Molecular weight
NaCl	125	58.44
KCl	2.5	74.55
NaH ₂ PO ₄ (H ₂ O) ₂	1.25	156.01
NaHCO ₃	26	84.01
CaCl ₂	2	110.98
MgSO ₄ (H ₂ O) ₇	1	203.3
D(+)-Glucose	10	180.16
O ₂ 95%	-	-
CO ₂ 5%	-	-

Attachment 11 : Internal solution

Chemical	mM	Molecular weight
K-Gluconate	136	234.25
KCl	6	74.55
(K)HEPES	10	238.30
(K)EGTA	0.5	
CaCl ₂	0.05	110.98
MgCl ₂ (H ₂ O) ₆	2	203.3
(Na) ₂ ATP(H ₂ O) ₃	4	605.26
(Na) ₂ GTP(H ₂ O) ₃	0.4	567.14
KOH	10	56.11

Attachment 12

Heatmap of the proportion of wakefulness observed at baseline in mice with expression of *AAV-EF1a-DIO-SSFO-EYFP* in AVP neurons ($n=9$). Each row represents one measurement, with the squares spanning 10-minute time bins. The fill color of squares represents the proportion of wakefulness within each 10-minute time bin and ranges from light blue (high proportion of wakefulness) to dark blue (low proportion of wakefulness). The x-axis gives Zeitgeber Time (ZT) measured as the number of hours after the lighting in home cages is turned on as an external cue (Zeitgeber).

Attachment 13

Heatmap of the proportion of wakefulness observed during, before and after stimulation of mice with expression of *AAV-EF1a-DIO-SSFO-EYFP* in AVP neurons ($n=9$). Each row represents one measurement, with the squares spanning 10-minute time bins. The fill color of squares represents the proportion of wakefulness within each 10-minute time bin and ranges from light blue (high proportion of wakefulness) to dark blue (low proportion of wakefulness). The x-axis gives Zeitgeber Time (ZT) measured as the number of hours after the lighting in home cages is turned on as an external cue (Zeitgeber). The white lines indicate the times of blue light exposure to the SCN.